Title Page

A Structural Heart-Brain Axis Mediates the Association Between Cardiovascular Risk and Cognitive Function

Akshay Jaggi,[1] Eleanor L.S. Conole,[2] Zahra Raisi-Estabragh,[3,4] Polyxeni Gkontra,[1] Celeste McCracken,[5] Liliana Szabo,[3] Stefan Neubauer,[5] Steffen E. Petersen,[3,4,6,7] Simon Cox,[2]* Karim Lekadir[1]*

[1] Facultat de Matemàtiques i Informàtica, Universitat de Barcelona, Barcelona

[2] Lothian Birth Cohorts, Department of Psychology, The University of Edinburgh, 7 George Square, Edinburgh EH8 9JZ, UK.

[3] William Harvey Research Institute, NIHR Barts Biomedical Research Centre, Queen Mary University of London, Charterhouse Square, London, EC1M 6BQ, UK

[4] Barts Heart Centre, St Bartholomew's Hospital, Barts Health NHS Trust, West Smithfield, EC1A 7BE, London, UK

[5] Division of Cardiovascular Medicine, Radcliffe Department of Medicine, University of Oxford, National Institute for Health Research Oxford Biomedical Research Centre, Oxford University Hospitals NHS Foundation Trust, Oxford, OX3 9DU, UK

[6] Health Data Research UK, London, UK

[7] Alan Turing Institute, London, UK

* Co-senior author

Corresponding Author:

Akshay Jaggi. Facultat de Matemàtiques i Informàtica, Universitat de Barcelona, Barcelona. Gran Via de les Corts Catalanes, 585, 08007 Barcelona, España.

Email: akshay.x.jaggi@gmail.com

Abstract

Elevated vascular disease risk associates with poorer cognitive function, but the mechanism for this link is poorly understood. A leading theory, the structural-functional model argues that vascular risk may drive adverse cardiac remodelling, which in turn leads to chronic cerebral hypoperfusion and subsequent brain structural damage. This model predicts that variation in heart and brain structure should associate with both greater vascular risk and lower cognitive function. This study tests that prediction in a large sample of the UK Biobank (N=11,962). We assemble and summarise vascular risk factors, cardiac magnetic resonance radiomics, brain structural and diffusion MRI indices, and cognitive assessment. We also extract 'heart-brain axes' capturing the covariation in heart and brain structure. Many heart and brain measures partially explain the vascular risk – cognitive function association, like left ventricular end-diastolic volume and grey matter volume. Notably, a heart-brain axis, capturing correlation between lower myocardial intensity, lower grey matter volume, and poorer thalamic white matter integrity, completely mediates the association, supporting the structural-functional model. Our findings also complicate this theory by finding that brain structural variation cannot completely explain the heart structure – cognitive function association. Our results broadly offer evidence for the structural functional hypothesis, identify imaging biomarkers for this association by considering covariation in heart and brain structure, and generate novel hypotheses about how cardiovascular risk may link to cognitive function.

Keywords: heart-brain axis, cognitive decline, cardiovascular disease, ageing, structural MRI, imaging-derived phenotypes

Introduction

With ageing populations throughout the world, cognitive decline now affects an increasingly large portion of society and contributes to significant financial burden and death (Gorelick et al., 2017; Wimo et al., 2013). Of the drivers of age-related cognitive decline, neurovascular health has gained attention due to its widespread impact and relative ease of intervention (Gorelick et al., 2011; Iadecola et al., 2016; Qiu & Fratiglioni, 2015; Sweeney et al., 2018).

Substantial work has shown diverse associations between vascular disease risk factors (VRFs, such as diabetes, high body mass index (BMI), and hypertension) and cognitive function (CF). Greater vascular risk in middle and old age associates with both poorer cognitive function and accelerated cognitive decline (Jefferson et al., 2010; Knopman et al., 2001; Lyall et al., 2017; Samieri et al., 2018; Yaffe et al., 2014), and controlling vascular risk factors can lead to a decrease in onset of mild cognitive impairment (SPRINT MIND Investigators for the SPRINT Research Group et al., 2019).

Better understanding of the mechanism of this heart-brain axis will facilitate biomarker development and treatment discovery for neurovascular health. Several mechanistic theories exist but lack evidence (Jensen et al., 2023; M. Wang et al., 2016; Zenger et al., 2023). One popular model, the structural-functional model, argues that VRFs might drive pathologic cardiac and cerebrovascular remodelling, which could then result in chronic cerebral hypoperfusion, brain structural damage, and poorer CF (de la Torre, 2012a, 2012b; Pasha et al., 2017; Qiu & Fratiglioni, 2015; van Buchem et al., 2014). Direct evidence for this theory has remained unclear but could be found by simultaneously measuring vascular risk factors, cognitive function, and heart and brain structure.

Cardiac and brain imaging derived phenotypes (IDPs) have become popular methods for measuring heart and brain structure due to their minimally invasive nature and widespread use. Both are strong candidate biomarkers of the modest but well-replicated association between elevated vascular risk and lower cognitive function in middle and older age (Ferguson et al., 2020; Lyall et al., 2017). However, to-date, most of our knowledge about associations between 1) VRFs, 2) cardiac structure, 3) brain structure, and 4) cognitive measures come from separate reports, which only simultaneously consider two phenotypes of interest (Cox, Lyall, et al., 2019;

Lyall et al., 2017; McCracken et al., 2021; Raisi-Estabragh, Jaggi, et al., 2021; Raisi-Estabragh, M'Charrak, et al., 2021). Several recent works have indicated the value in extending analyses across three of the four phenotype categories above (Bai et al., 2020; McCracken et al., 2022; Newby et al., 2021; Shen et al., 2020); for example, lower grey matter volume can explain part of the association between hypertension, greater BMI, and lower performance on some UK Biobank cognitive exams (Ferguson et al., 2020). Most recently, a large scale study has revealed that cardiac imaging features, brain imaging features, and neuropsychiatric disease all share a common genetic influences, motivating further work in exploring how these systems may interact physiologically (Zhao et al., 2023). However, none of these studies have specifically studied how inter-relations between cardiac and brain structural variation could explain the vascular risk - cognitive function association.

We hypothesise that, for the structural-functional model to adequately explain the VRF-CF association, separate heart and brain structures should associate with both greater vascular risk and lower cognitive function. In other words, heart and brain structural variation should mediate the VRF-CF association (Bai et al., 2020; McCormick et al., 2022). Additionally, heart mediators should associate with brain mediators. Finally, for all steps of the structural-functional model to be supported by the data, heart structural variation should mediate the VRF - brain structure association, and brain structural variation should mediate the heart structure - CF association. The extent to which these associations all align in a cohort of subjects modelled together is understudied (Ferguson et al., 2020; Gorelick & Sorond, 2018; Newby et al., 2021). Furthermore, the relative strength of the association between cardiac and brain structural features and the disease endpoints (vascular risk and cognitive decline) is unknown. Along with validating the structural functional hypothesis, this comparative approach could identify novel biomarkers associated specifically with the VRF-CF association (rather than each dataset alone) and guide future decision-making comparing and prioritising organ-specific interventions in vascular and cognitive health (Banus et al., 2021; Gorelick et al., 2011, 2017; Gorelick & Sorond, 2018).

To test the structural-functional hypothesis, in this work, we measure the extent that variation in heart and brain structure explains the association between vascular risk and cognitive function in the UK Biobank. We gather vascular risk factors, cognitive exam performance, cardiac magnetic

resonance imaging (CMR) radiomics features, and brain MRI IDPs for 11,962 UK Biobank participants. We perform dimensionality reduction on all datasets separately. We discover novel measures of the heart-brain axis by capturing correlated variance in heart and brain imaging. We compute single and multiple mediation models asking how well imaging latent variables explain the VRF - CF association. We then measure how well imaging latent variables explain associations between individual VRFs and cognitive exams. We finally explore how well individual heart and brain structural measures mediate the VRF - CF association. Along with myriad smaller mediating effects, we find that myocardial intensity, grey matter volume, and thalamic white matter tract integrity all associate with each other, and a joint factor capturing their variability most strongly associates with both elevated vascular risk and poorer cognitive function.

Methods

Acquisition and Processing

Assessment

This work utilises clinical and imaging data from the United Kingdom (UK) Biobank via access application 2964 (Ukbb-Prot-, n.d.). The UK Biobank is a large-scale longitudinal dataset derived from 500,000 volunteers recruited between 2006 and 2010 from across the UK. At visits, participants completed both a touchscreen questionnaire and medical history interview with a nurse. The project recorded information regarding participants' health, lifestyle, and family history and collected physical measurements, biological samples, and genome. Moreover, since 2015, over 50,000 participants have received CMR and brain MR imaging at followup imaging visits.

Vascular Risk Factors

We analysed hypercholesterolemia, diabetes, hypertension, smoking pack years, blood pressure, and anthropomorphic measures (BMI and waist-to-hip ratio, WHR) (Cox, Lyall, et al., 2019; de

la Torre, 2012a, 2012b; Haley et al., 2018; Pasha et al., 2017; Sweeney et al., 2018). All vascular risk factors were collected at the baseline visit and prepared as reported previously (Cox, Lyall, et al., 2019; Raisi-Estabragh, Jaggi, et al., 2021). We summarise the process here. Diagnosis of diabetes, hypertension, and hypercholesterolemia was established via a combination of self-report, biochemistry, and linked hospital episode statistics (HES) data (**Supplementary Methods**) (Raisi-Estabragh, Jaggi, et al., 2021). Participants provided information on cigarette smoking in the touchscreen questionnaire, and smoking pack years were computed from this data (Cox, Lyall, et al., 2019). Blood pressure was collected twice, moments apart, using an Omron 705IT monitor. Mean systolic and diastolic blood pressure were computed. Anthropometric measures were taken after participants had removed bulky clothing and shoes. Waist and hip measurements were conducted to provide WHR. BMI was computed by dividing weight by squared height.

Cognitive Exams

Cognitive testing was performed at both the UK Biobank baseline and imaging sessions; we examined four tests from the imaging visit cognitive assessment. The complete battery and assessment of its repeatability and reliability have been detailed previously (Fawns-Ritchie & Deary, 2020; Lyall et al., 2016, 2017). We used the four tests commonly used in analysis and dimensionality reduction of the baseline cognitive assessment: the fluid intelligence task (verbal numerical reasoning, VNR), the visual memory task (vismem), the reaction time task (RT), and the prospective memory task (prosmem) (Lyall et al., 2016). As previously reported (Lyall et al., 2016), the reaction time scores were positively skewed, so we applied a natural log transformation (LN). Additionally, the visual memory scores were zero-inflated and positively skewed, so we applied a LN+1 transformation.

Cardiac Imaging

Cardiac imaging acquisition and preparation discussed in **Supplementary Methods**. Using the CMR images and their corresponding segmentations, we performed radiomics phenotyping based on the open-source python-based pyradiomics library (van Griethuysen et al., 2017). Radiomics extracts features quantifying myocardial and ventricular structure (shape radiomics), myocardial imaging intensity (first-order radiomics), and myocardial visual textures (texture

radiomics) (Raisi-Estabragh et al., 2020). In total, 212 features per region were extracted at end-diastole and end-systole. Right and left ventricular cavity first-order and texture features were excluded from analysis because they do not encompass clinically relevant information. We also incorporate alternative traditional and advanced CMR indices into the matching analysis and final mediation by individual features, computed as previously reported (detailed in **Supplementary Methods**) (Bai et al., 2020; McCracken et al., 2021; Raisi-Estabragh, McCracken, et al., 2021; Raisi-Estabragh, M'Charrak, et al., 2021; Zhao et al., 2023).

Brain Imaging

Brain imaging acquisition and preparation is discussed in **Supplementary Methods**. The global tissue volumes and white matter tract-averaged water molecular diffusion indices were processed by the UK Biobank team and made available to approved researchers as imaging-derived phenotypes (IDPs); the full details of the image processing and QC pipeline are available in an open access article (Alfaro-Almagro et al., 2018). The IDPs in this study included total brain volume, grey matter volume, subcortical volumes, and tract-averaged white matter microstructural measures. A detailed list of volumes, white matter tracts, and white matter tract measures is provided in **Supplementary Methods**.

Analysis

Workflow

We began with 19408 subjects with completed CMR radiomics analysis of their short-axis imaging from the UK Biobank Imaging Extension. We downloaded and prepared the vascular risk factor, cognitive testing, brain imaging data, heart imaging, and covariates for these subjects (see Acquisition and Preparation). For each dataset separately, we dropped all subjects without complete data, merged all datasets, and selected only subjects without cardiovascular or brain disease (defined in **Supplementary Methods**). We then performed dimensionality reduction on each data type separately. We performed joint factorization of the heart and brain imaging data. We regressed out imaging confounders from the latent factors (**Supplementary Methods**). We merged the latent factors and performed all downstream analyses. We corrected all comparisons

for multiple hypothesis testing with a Benjamini-Hochberg False Discovery Rate (BH-FDR) correction. Entire pipeline with number of subjects retained at each step reported in **Supplementary Figure 1** and population statistics reported in **Supplementary Table 1**. For every analysis, we present both raw and deconfounded results as paired **Supplementary Tables**, but we only discuss deconfounded results in the text. All code was open-sourced, see **Data and Code Availability**; the list of packages and settings used is in **Supplementary Methods**.

Dimensionality Reduction

Latent Variables for Vascular Risk (gVRF)

First, we derived an aggregate measure of vascular risk for each individual, counting instances of diagnosis of hypertension, diabetes, or hypercholesterolaemia, having ever smoked, having a BMI >25, and having a high WHR (>0.85 for females and >0.90 for males) (Cox, Lyall, et al., 2019; Hamer & Batty, 2019). This factor is useful for clinical translation and also defining simple high and low risk groups.

We derived an additional latent factor of general vascular risk (gVRF) following prior work in this and other cohorts, using confirmatory factor analysis (CFA) in structural equation modelling (Cox, Lyall, et al., 2019; Wardlaw et al., 2014). This latent measure captures the tendency for VRFs to co-occur. gVRF was derived from smoking pack years, diastolic and systolic blood pressure, BMI, WHR, diagnosis of hypertension, diabetes and hypercholesterolaemia. The model fit the data well, though loadings were inconsistent (range 0.189–0.745), with the factor more strongly loaded towards BMI and WHR (**Supplementary Figure 2, Supplementary Table 2**). Because the aggregate measure of vascular risk relies on arbitrary cutoffs and there is high correlation between the aggregate measure and gVRF, we focus on gVRF in our discussion of all mediation analyses.

Latent Variables for Cognitive Function (general intelligence, g)

As previously reported (Lyall et al., 2017), we performed a CFA of the four cognitive tests. We hypothesised that the four tests would correlate moderately-highly (with intercorrelations of $r > 0.40$) and would form a single latent general factor (labelled g in prior literature) across the four

tests with good fit to the data (Cox, Ritchie, et al., 2019; Deary et al., 2010; Lyall et al., 2016). We found this to be the case (**Supplementary Figure 3, Supplementary Table 3**).

Latent Variables for Heart Structure

Since principal component analysis (PCA) is commonly used in radiomics to extract lower dimensional representations of the data (Antonopoulos et al., 2021; Raisi-Estabragh et al., 2020; Truhn et al., 2019; Zhang et al., 2017), we performed PCA on the z-scored radiomics. We chose the number of principal components using cross validation, detailed in the **Supplementary Methods**. We kept the first 3 unrotated PCs (**Supplementary Figure 4, Supplementary Table 4**). We extracted the scores of these components for each subject and used them for downstream analyses.

Latent Variables for Brain Structure

We isolated brain volume ('atrophy' after controlling for head size), grey matter volume, and total white matter hyperintensity volume (Cox, Lyall, et al., 2019). Latent measures of general white matter fractional anisotropy (gFA) and mean diffusivity (gMD) were derived using CFA, as previously reported in this cohort (Cox et al., 2016; Cox, Lyall, et al., 2019). The CFA models fit well with the lowest loadings for the corticospinal tracts and cingulate gyri and the highest loadings for the thalamic radiata and fasciculi (**Supplementary Figure 5, Supplementary Table 5**) .

Since principal component analysis has been used to capture variation in brain imaging in previous work and since we are using it to summarise the heart imaging in this work (Alfaro-Almagro et al., 2021; Elliott et al., 2018; Liang et al., 2021; Miller et al., 2016), we also computed PCA over all z-scored brain IDPs and selected the number of principal components to retain as before (**Supplementary Methods**). We kept three PCs (**Supplementary Figure 6, Supplementary Table 6**). We extracted their scores for each subject and utilised them in downstream analyses. Because both CFA and PCA are widely used in the field and there is no definitive reason for preferring one to the other, we will include both in all downstream analyses to ensure that our findings are not dependent on the method of latent feature definition (John et al., 2012).

Joint Heart-Brain Factor Analysis

Along with the factor analysis of the individual datasets described above, we also sought to derive latent factors that captured the main modes of correlated variation between heart and brain structural imaging. That is, we aimed to identify components of brain structure and components of heart structure that were maximally correlated. Through canonical correlation analysis (CCA) on the z-scored heart radiomics and brain IDPs, we derived ten modes (Miller et al., 2016). Each mode consists of two components: (1) a linear combination of heart radiomics features and (2) a separate linear combination of brain IDPs that have highly similar variation in the population. The modes are ranked by the amount of correlation between the heart and brain components. We chose the number of modes to keep via cross validation (**Supplementary Methods**), kept three modes (**Supplementary Figure 7, Supplementary Table 7**), extracted the component scores for each subject in each dataset, and used them in downstream analyses.

Descriptive Statistics and Associations

We conducted descriptive analyses, testing the association of age and sex with all of our latent variables using linear regression. We then examined the pairwise linear association between all latent variables by linearly modelling each latent variable as a function of sex, age, and each other latent variable. See **Supplementary Methods** for modelling details and how additional R^2 is computed. Results reported for both raw and deconfounded imaging latents.

Propensity Score Matching

Since all other analyses are performed on corrected, standardised, and latent measures of the data, we performed propensity score matching to yield real-units measurements of the differences between subjects with and without VRFs. We matched subjects with four or more VRFs with their nearest neighbour with no VRFs, requiring an exact match for sex (**Supplementary Methods**). We then performed repeated t-tests to compare the cognitive exam performance, CMR measures, and brain IDPs of the matched groups of subjects.

Mediation Modelling

To measure how well heart and brain structural features explain the VRF-CF association, we perform a series of mediation analyses (Bai et al., 2020; Ferguson et al., 2020; McCormick et al., 2022; Wardlaw et al., 2014). This method allows us to directly quantify the degree to which any identified associations between vascular risk and cognitive function are accounted for by brain or heart-based measures. The primary outcome is therefore the % of the gVRF-g association that is mediated when brain/heart measures are included in the model. In more complex models with more than one mediator, one can also identify which mediator is contributing the largest unique mediating effect. Thus, these analyses offer an elegant quantitative solution for identification of important heart and brain biomarkers underpinning VRF-cognitive associations. We report a more complete description of the mediation model in the **Supplementary Methods**.

We first performed mediation models on solely the latent representations of each data set. We found the association between gVRF and g and then modelled how well each imaging latent variable mediated this association (more details in **Supplementary Methods**). At first, we only modelled one imaging latent at a time, calling this the 'Latent Single Mediation Model.' Then we performed both parallel and sequential multiple mediation analyses, fixing heart PC2 as the first mediator and then adding brain latents as the second mediator, called 'Latent Multiple Mediation Model.' Next, we replaced the gVRF-g association with pairs of individual VRFs and cognitive exams, testing imaging latents one at a time again, calling this 'Latent Single Mediation Modelling of VRF-Cognitive Pairs.' Given the high association between the VRFs (**Supplementary Figure 2, Supplementary Table 2**), we control each VRF-exam association for all other VRFs to identify unique associations between each VRF and cognitive exam.

To explore the role of individual imaging features in explaining the association between VRFs and CF, we returned to the gVRF-g association and performed mediation modelling for each imaging feature individually, calling this the 'Individual Feature Single Mediation Model.' We perform modelling as described in **Supplementary Methods** and always control for age and sex.

Given that all latent measures across domains (vascular risk, heart, brain and cognitive) were standardised, reported coefficients are standardised regression coefficients (i.e. β range [-1 ,1]) throughout, allowing direct comparison of effect magnitudes across modalities.

Results

Quantifying Heart Brain Axes

After our data preparation pipeline yielded 11,962 subjects (**Supplementary Figure 1, Supplementary Table 1**), we quantified key axes of variation in all four of our datasets. We extracted latent measures of vascular risk (gVRF), cognitive function (g), and brain structure as reported previously (see **Methods**) (Cox, Lyall, et al., 2019; Cox, Ritchie, et al., 2019; Ferguson et al., 2020; Lyall et al., 2016, 2017). Along with traditional measures, we performed PCA of heart and brain imaging separately and a novel CCA to capture correlated variability in heart and brain structure (**Figure 1**). For cardiac radiomics, the first three PCs explain 25, 20, and 12% of the variance and represent myocardial size, intensity, and textural complexity respectively (**Supplementary Figure 4, Supplementary Table 4**). For brain MRI indices, the first three PCs explain 30, 12, and 8% of the variance and represent high FA and low MD of the fasciculi and thalamic radiata, high FA and low MD of the corticospinal tract, and brain volume respectively (**Supplementary Figure 6, Supplementary Table 6**). For the joint heart brain axes, the first three modes have a Pearson correlation of 0.71, 0.48, and 0.32 respectively (**Supplementary Figure 7, Supplementary Table 7**). Based on the loadings, we interpreted that the heart brain axes correspond to 1) heart and brain volume, 2) end-systolic myocardial intensity, grey matter and thalamic volume, and thalamic radiation WM integrity, and 3) end-diastolic myocardial intensity and low FA and high MD of many tracts (more details in **Supplementary Methods**).

Descriptive Statistics

Nearly all latent variables have a significant association with age and sex (**Supplementary Figure 8, Supplementary Tables 8, 9**). Older subjects show lower aggregate performance on cognitive exams (β=-0.183) and greater vascular risk (β=0.171) (Cox, Lyall, et al., 2019; Lyall et al., 2017). Among the heart structural latents, old age associates with slightly greater myocardial volume (CMR PC1, β=0.035), lower myocardial intensity (PC2, β=-0.173), and lower myocardial textural complexity (PC3, β=-0.109) (Rouch et al., 2022).

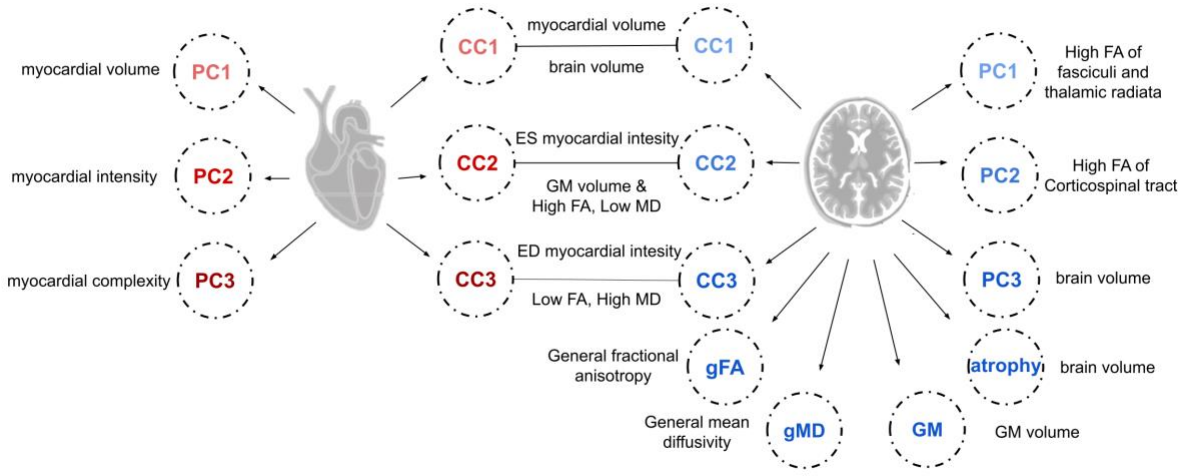

Figure 1: Latent Factors

A schematic illustrating all of the extracted latent factors and a simple interpretation of their meaning. The loadings for all the factors can be found in the **Supplementary Tables** and more detailed interpretations of the meaning of each factor can be found in the **Supplementary Methods**.

Among the brain structural latents, old age associates with lower total and grey matter volume, lower white matter integrity (β range -0.363 to -0.249), and greater white matter hyperintensity volume (β=0.353). Age also strongly negatively associates with the components of the second CCA mode, representing lower myocardial intensity, grey matter and thalamic volume, and thalamic white matter integrity (β range -0.591 to -0.441).

Associations Between Vascular Risk, Heart, Brain, and Cognition

Associations among each pair of latent variables were modelled separately, controlling for age and sex (**Figure 2, Supplementary Tables 10, 11**). There is a small but significant negative association between gVRF and g (β=-0.036), consistent with prior reports (Ferguson et al., 2020; Lyall et al., 2017). Many imaging latents across heart and brain associate with both greater gVRF and lower g: lower latent myocardial intensity, lower total and grey matter volume, lower white matter tract integrity, and greater white matter hyperintensity volume. (**Figure 2, Supplementary Table 11**).

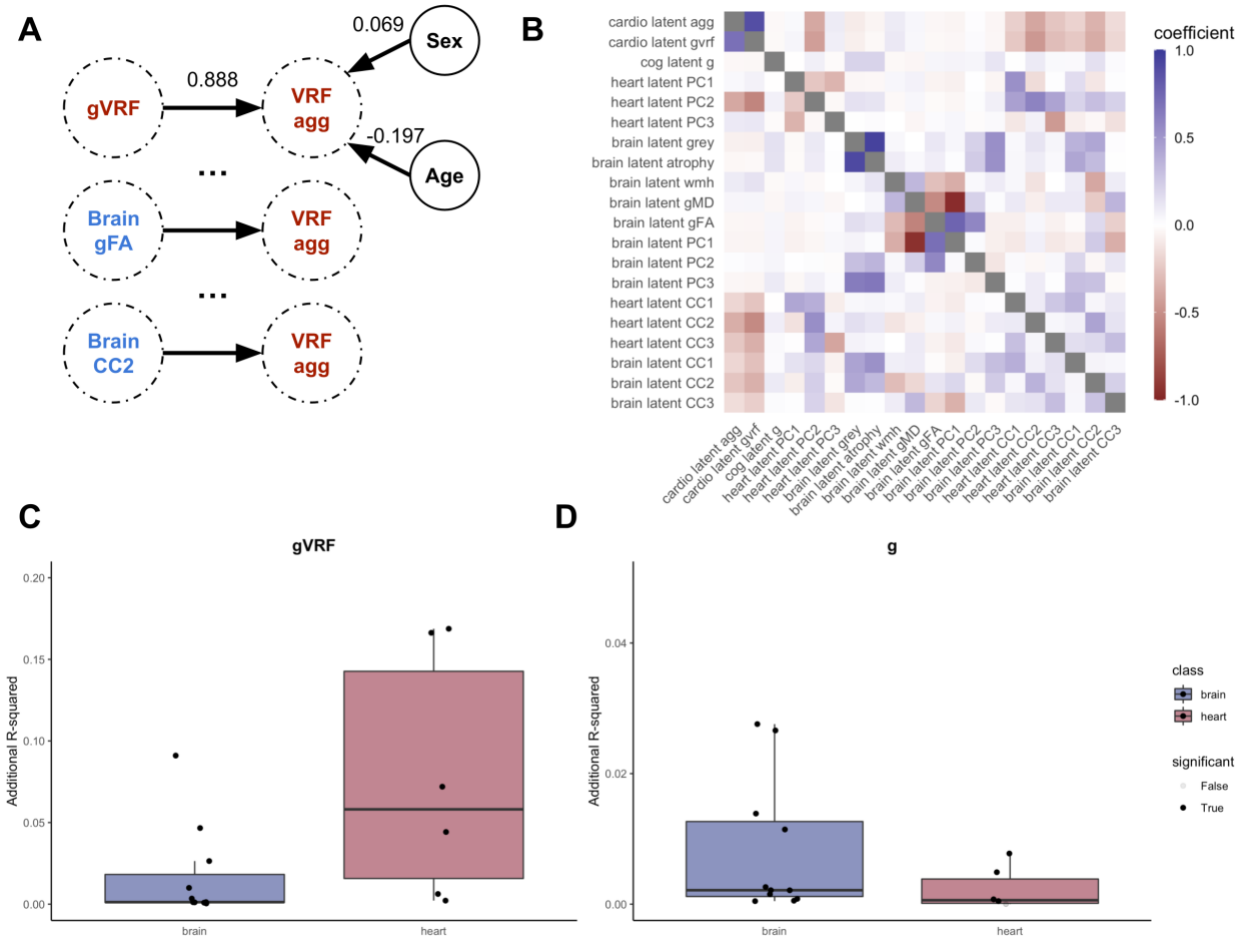

Figure 2: Pairwise Latent Associations

We modelled the association between every pair of latent variables. (A) A schematic diagram of the modelling process. Every latent variable (e.g.VRF agg) is linearly modelled as a function of another latent variable (e.g. gVRF), sex, and age. The derived coefficients for the example first model are illustrated. We repeat this for every variable, and the coefficient from these analyses compose the first row of the adjacent heatmap. (B) Heatmap of standardised coefficients from all 342 separate pairwise linear models. Each row lists the dependent variable, and each column lists the independent variable in the linear models. (C) With gVRF set as the dependent variable, we compare the R-squared of the linear model for each latent grouped by whether it was derived from the heart or brain imaging. (D) With g set as the dependent variable, we compare the R-squared of the linear model for each latent grouped by whether it was derived from the heart or brain imaging. All model estimates reported in **Supplementary Table 11**.

All of the heart PCs explained at least an order of magnitude more variance in gVRF (additional R^2: 0.002–0.166) than in g (aR^2: 0–0.004) (**Figure 2**). Similarly, the brain volume latents (atrophy, grey matter volume, PC3) explained at least an order of magnitude greater variance in g (aR^2: 0.012–0.027) than in gVRF (aR^2: 0.0006–0.003). Interestingly, the second joint factor (CC2) explains more similar amounts of variance in both g (aR^2: 0.009–0.013) and gVRF (aR^2: 0.089–0.164), and it explains at least an order of magnitude more variance in both g and gVRF than the white matter latents. This suggests that leveraging information from both heart and brain structure is useful in deriving factors that explain a relatively large and equal amount of variance in both vascular risk and cognitive function.

Matched Analysis

Aware that the latent measures are all in arbitrary units, we used propensity score matching to provide more practically interpretable information on how those with high and low vascular risk differ across heart, brain and cognitive measures, in native units. We assembled two groups of 425 subjects matched by sex, age, head size, and BSA (**Supplementary Table 12**). On average, when compared to matched individuals with no VRFs, subjects with 4 or more VRFs have 13.09 mL (8.29%) lower LVEDV, 7.56 mL (11.50%) lower LVESV, and 5.52 mL (5.99%) lower LVSV. Consistent with mild ventricular hypertrophy, the subjects with 4 or more VRFs have 1.51% (2.58%) greater ejection fraction. We find lower average intensities of the myocardium in end- systole (23.53%) and diastole (19.65%). We also find greater uniformity of the myocardial tissue appearance (5.25–8.37%). These subjects also have 14,357 mm^3 (2.31%) less grey matter volume and additionally lower subcortical volumes. They have greater white matter hyperintensity volume (62.34%). They also have lower FA in many tracts (range 0.96% and 1.92%). Compared to matched healthy controls, subjects with 4 or more VRFs also score on average 0.48 (6.67%) fewer points on verbal-numerical reasoning. These subjects also have notable differences in their latent measures, like greater myocardial size, poorer white matter tracts, and lower second heart-brain axis (myocardial intensity, grey matter volume, thalamic WM tract integrity). Simply summing risk factors correlates with gVRF (**Figure 2, Supplementary Table 11**), and this matched analysis shows that the sum manifests with

clinically observable phenotypes in heart imaging, brain imaging, and cognitive exam performance.

Latent Single Mediation Modelling

Initially, we asked the degree to which each brain or heart measure, in isolation, mediates the association between vascular risk and CF. Results are presented in **Figure 3**, **Supplementary Tables 13, 14.** Consistent with prior reports, measures of brain structure - irrespective of how they were measured - only modestly mediated the association (4.97–38.12%), with white matter measures being the smallest, but still significant, mediators. However, latent myocardial intensity (heart PC2) and the heart-brain axis capturing myocardial intensity, grey matter volume, and thalamic white matter integrity (CC2) all completely mediate the gVRF-g association (117%-150%; attenuated to be indistinguishable from β =0 in each case). For example, one standard deviation (SD) lower gVRF associates with 0.55 standard deviation lower latent myocardial intensity. This 0.55 SD lower intensity associates with 0.043 SD lower cognitive function.

As a control, we address two possible counterarguments: (1) that the BMI - cognitive function association is the only VRF well explained by myocardial intensity and (2) that latent myocardial intensity is just a proxy for myocardial size. First, since gVRF most strongly weights BMI and WHR (**Supplementary Table 2**), it's possible that the gVRF-g association is driven primarily by BMI and that latent myocardial intensity only mediates the BMI - g association. However, covarying for BMI partly attenuated, but did not remove, myocardial intensity's mediation of the gVRF-g association (40.18%) (**Supplementary Table 15**). Second, since latent myocardial intensity and myocardial volume are associated (**Supplementary Table 11**), it is possible that latent myocardial intensity is just a measure of myocardial size not well adjusted by regressing out BSA. However, we show that latent myocardial intensity associates with BMI independent of body and myocardial size (**Supplementary Table 15**). Therefore, latent myocardial intensity's mediation of the gVRF-g association is not just explained by the BMI - g association and, furthermore, the BMI - latent myocardial intensity association is not just due to the myocardium being larger.

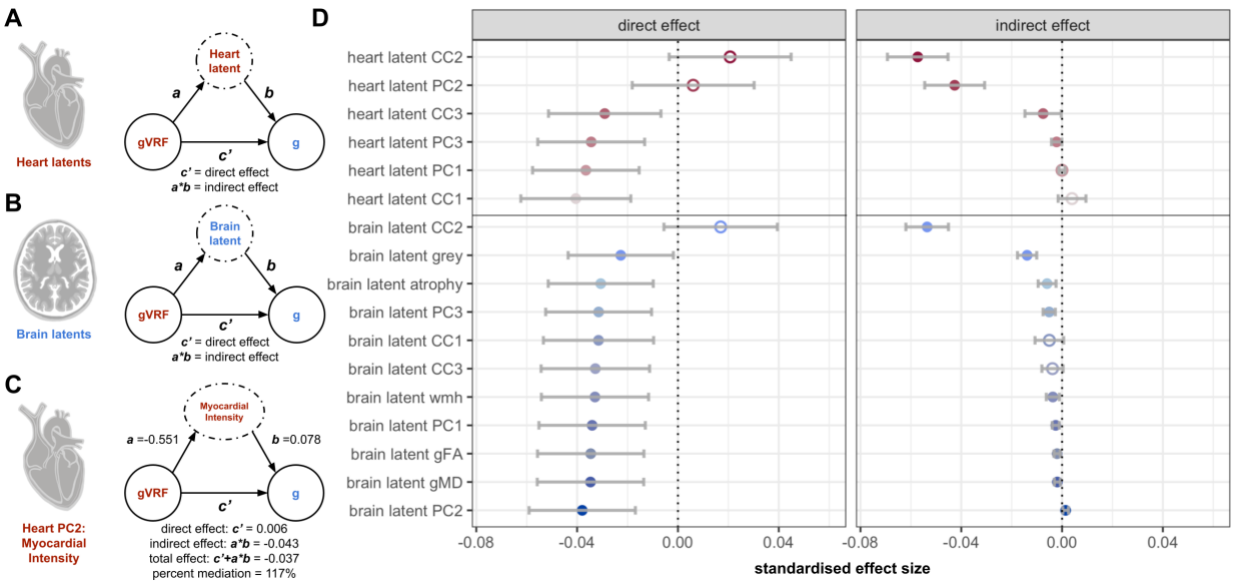

Figure 3: Latent Single Mediation Modelling

We performed serial mediation modelling of the gVRF-g association, testing each imaging latent as a potential mediator. (A) Schematic for the CMR radiomics modelling procedure. gVRF and g were maintained as the known association, and we iterated over all CMR imaging latent factors. Equations demonstrate the derivation of the direct and indirect effect. (B) Schematic for the brain MRI modelling procedure. (C) Example computation of the measured effects. Confidence intervals reported in **Supplementary Table 14**. (C) The estimates for the direct and indirect effects for all potential mediators, sorted by indirect effect size, closed circles are significant ($p<0.05$) and open are not. Error bars derived from bootstrapping (see **Supplementary Methods**).

Latent Multiple Mediation Modelling

The structural functional model argues that heart structural variation impacts cognitive function via its impact on brain structure. To model this within our data, we constructed two related multiple mediation models (**Figure 4**). In the first model, we performed 'parallel' multiple mediation that does not account for the heart-brain association. In the second model, we performed 'sequential' multiple mediation that does account for the heart-brain association.

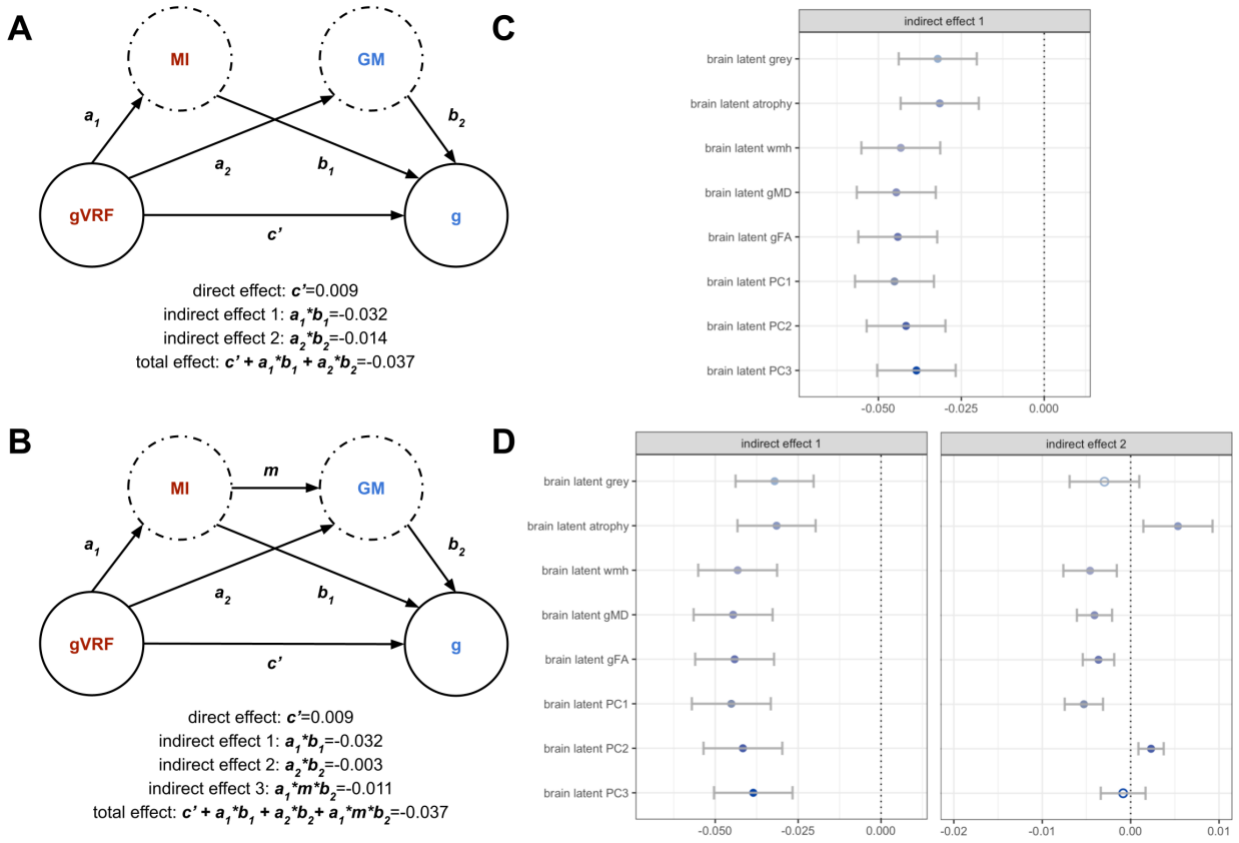

Figure 4: Latent Multiple Mediation Modelling

We performed both parallel and sequential multiple mediation modelling of the gVRF-g association, including heart PC2 as the first mediator and then considering all brain latents as second mediators. (A) Schematic of the parallel modelling procedure with a single direct effect and two indirect effects, one for each potential mediator. We list values from an example mediation effect in which grey matter volume was the second mediator. Confidence intervals reported in **Supplementary Table 17**. The direct effect is fixed for all mediators at 0.009. (B) Analogous schematic for the sequential modelling procedure. Values reported from an example model with grey matter as the second mediator. **Full data in Supplementary Table 19**. (C) A bar chart of the estimates for the indirect effect for heart PC2 when each brain latent was used, closed is significant ($p<0.05$) and open is not. (D) A bar chart of the estimates for the indirect effect for each brain latent when either using parallel (left) or sequential (right) mediation.

We performed this analysis for latent myocardial intensity paired with every brain latent since latent myocardial intensity was the only significant heart mediator. Comparing the heart indirect effects between the single mediation (**Figure 3**) and the parallel multiple mediation (**Figure 4C, Supplementary Tables 16, 17**) allows us to assess the impact of brain structure on the heart-cognitive function association. The heart indirect effect slightly decreases when accounting for brain volumes but not brain white matter measures. Therefore, brain volume variation can explain some but not all of the association between latent myocardial intensity and cognitive function. Comparing the brain indirect effects between the parallel and sequential mediation allows assessment of the impact of latent myocardial intensity on the VRF-brain association. In this case, the brain volume measure indirect effects go to zero but the white matter indirect effects do not decrease (**Figure 4D, Supplementary Tables 18, 19**). Thus, latent myocardial intensity variation can explain all of the association between VRFs and brain volume but not VRFs and white matter intensity.

Latent Single Mediation Modelling of Individual VRF-Cognitive Pairs

Recent work has noted the potential for spurious mediations when modelling with composite measures; for example, false 'interrupted mediators' occur when one component of a composite mediator associates with only the causal variable and one component associates with only the outcome. To confirm that our results are robust to this concern, we spend the next two sections analysing mediation using individual measures. We first consider pairs of individual VRFs and cognitive exams (**Supplementary Figure 9, Supplementary Tables 20, 21**). We found that pack years and VNR (β =-0.028), WHR and VNR (β =-0.061), and WHR and RT (β =0.032) all had independent associations in the expected directions. Brain volumetric latents most strongly mediated the pack year - VNR association (12.11–47.64%) while myocardial intensity associated latents most strongly mediated the WHR-VNR association (27.33–42.76%). The myocardial intensity features are also the only significant mediators of the WHR-RT association (34.75–49.52%). Likely because they capture some relevant variation in brain volumes, white matter tracts, and myocardial intensity, the components of the second joint factor strongly mediate both the pack-year and WHR cognitive exam associations (21.63–49.52%).

Individual Feature Mediation Modelling

Continuing our controls for spurious mediation from composite measures, we next turn to individual imaging measures. Although the latent imaging features capture large amounts of the variance in the imaging datasets (**Supplementary Figure 4, Supplementary Figure 6**), each imaging dataset contains many features and much variance beyond the latents used in the previous analyses. To offer a comprehensive picture of how heart and brain structure mediate the gVRF-g association, we perform single mediation analysis for every individual imaging feature (**Figure 5, Supplementary Tables 22, 23, 24, 25**).

As expected, many individual features associated with myocardial intensity show complete mediation (**Figure 5, Supplementary Tables 22, 23**). However, a number of CMR measures showed mediating effects that were previously difficult to appreciate via latent modelling. While the latent measure of myocardial volume did not mediate the association (**Figure 3**), both the right and left ventricular volumes partially mediated the association (32.5–61.1%). Although the latent measure of myocardial tissue complexity was just below significance (**Supplementary Table 14)**, some measures of local nonuniformity and local homogeneity partially mediated the association (32.5–48.5%). Greater local nonuniformity associated with lower vascular risk (β = -0.347– -0.284) and greater cognitive function (β = 0.051–0.054), and measures of local homogeneity show the opposite associations (**Supplementary Table 23**).

Compared to the heart, the brain IDPs show an order of magnitude lower indirect effects and proportionally lower percent mediation (**Figure 5, Supplementary Tables 24, 25**). Of the brain IDPs, volumes have the largest mediating effect, particularly grey matter (38.1%) and thalamic volume (35.9–36.4%). The largest white matter microstructural mediating effects are from the thalamic radiation tracts (**Supplementary Figure 10**). For example, MD of all the thalamic radiation tracts significantly mediates the association (5.17–8.26%), and the FA of the left posterior thalamic radiation tract has the greatest mediation of all the white matter microstructural mediating effects (18.3%).

For both the VRF-Cognitive exam pairs and the individual mediators, the existence of significant mediation for individual features argues against potential spurious mediation due to composite measures (McCormick et al., 2022).

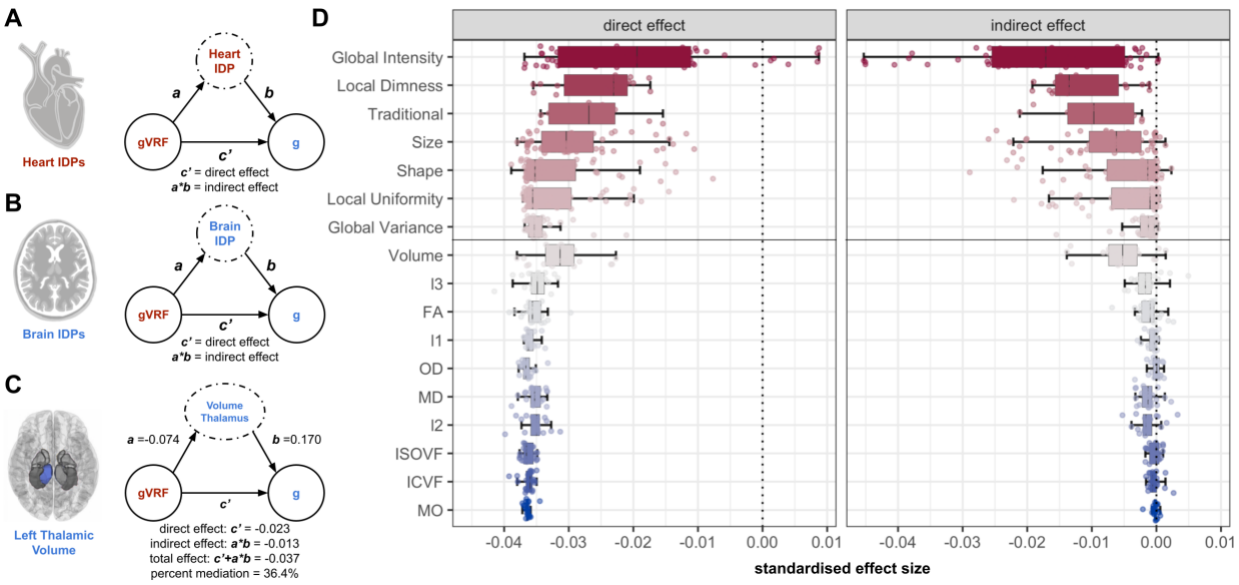

Figure 5: Individual Feature Single Mediation Modelling

We performed serial mediation modelling for all individual imaging features. (A) Schematic for the modelling procedure for CMR IDPs. Same as **Figure 3**, except all potential mediators are now individual features (IDPs) instead of latent variables. (B) Schematic for Brain IDPs. (C) Example mediation model for an individual feature with the left thalamic volume (Volume Thalamus) as a potential mediator. Confidence intervals reported in **Supplementary Table 25**. (D) Direct and indirect effects for all tested CMR radiomics grouped by cluster and brain MRI IDPs grouped by their feature type. For visualisation, we grouped the brain IDPs by their IDP categories and the CMR radiomics by previously reported clusters extracted from imaging of healthy individuals (Raisi-Estabragh, Jaggi, et al., 2021). We also include conventional CMR indices as a separate cluster.

Lastly, we considered whether an expanded set of CMR indices including myocardial strain, myocardial thickness, aortic dilation, and other advanced shape-based features could mediate the vascular risk - cognitive function association (Bai et al., 2020; Zhao et al., 2023). After controlling for body surface area, none of these advanced shape measures are significant mediators of the vascular risk - cognitive function association (**Supplementary Table 26**).

Discussion

Interpretation

This study supports the structural-functional model for the link between vascular risk and cognitive function. Many heart and brain structural measures separately mediate the vascular risk - cognitive function association (**Figure 3, 6**). Despite these initial results, it was still possible that the mediating measures from the heart and brain shared no inter-associations. This would violate the structural-functional model's claim that vascular risk causes vascular and cardiac remodelling, which in turn causes cerebral damage. Our results argue against this possible negative result in three ways. First, we find significant associations among the separate heart and brain mediators, like between heart PC2 and grey matter volume (**Figure 2**). Second, we find that these associated mediators have partially overlapping mediating effects (**Figure 4**). Third, we find that one of the major axes of covariance between heart and brain structure (CC2) significantly mediated the VRF-CF association (**Figure 3**). Therefore, the heart and brain do indeed share mediating effects, indicating that their variation may be linked via the structural-functional model.

Our results also complicate the structural functional model. When comparing the multiple mediation models (**Figure 4**), we found that latent myocardial intensity variation can fully explain the VRF-grey matter association, but grey matter variation cannot fully explain the latent myocardial intensity - cognitive function association. This suggests that heart structural variation can associate with cognitive function in ways independent of brain structural variation. This violation of the structural functional model could be explained by brain changes not well captured by our metrics (e.g. smaller cortical grey matter changes). Additionally, we found that latent myocardial intensity cannot explain the VRF-white matter integrity association (**Figure 4**). Therefore, the brain associates with risk factors in manners independent of cardiac variation. Mechanisms for this break in the model could be explained by direct impact of metabolic hormonal dysregulation on the brain or brain vasculature, without affecting heart structure.

Consistent with prior reports, considering brain structural measures alone only accounted for a minority of the VRF-CF association (Ferguson et al., 2020). Although important features from

these brain latents all have relatively large coefficients in the second heart-brain CCA mode (**Supplementary Table 7**), these latents alone show much smaller indirect effects than the second heart-brain CCA mode (**Supplementary Table 14**). The strong alignment of the second CCA mode with the VRF-CF association suggests that leveraging the association between heart and brain structure is informative to deriving a brain imaging latent factor that associates with both vascular risk and cognitive decline. In other words, without considering vascular risk or cognitive function in their derivation, one can discover brain biomarkers that better explain the VRF-CF association by using the heart-brain structural association.

Focusing on the brain structures identified, this work unifies separate findings that have shown that lower grey matter and thalamic volume associates with greater vascular risk and lower cognitive function (Bai et al., 2020; Cox, Lyall, et al., 2019; Cox, Ritchie, et al., 2019; Ferguson et al., 2020). Furthermore, this work supports the association of deteriorating thalamic tract white matter microstructure with elevated vascular risk and poorer cognitive function (Cox, Lyall, et al., 2019; Cox, Ritchie, et al., 2019). Previous work has argued that the thalamus is both central to integrative signalling in the brain and potentially susceptible to changes in cerebrovascular perfusion (Bohlken et al., 2014; Cox et al., 2016; Payabvash et al., 2011; Rikhye et al., 2018). Crucially, this works links variation in these structures to myocardial intensity. Why exactly thalamic volume and thalamic white matter integrity associate with myocardial intensity is still unknown and will be of interest in future work.

Our analyses of individual VRFs and cognitive exams revealed subtle trends not apparent in our more global/latent results, where brain and heart had differential importance. For example, whereas brain volumes more strongly mediate the pack year - VNR association than the WHR-VNR association, myocardial intensity exhibited the reverse pattern (**Figure 5, Supplementary Table 21**). This result highlights the utility of a comparative approach between heart and brain structural variation. However, the individual VRF cognitive exam analysis also revealed the complexity in some of these phenotypes, replicating a previous finding of a positive association between BMI and visual memory (**Supplementary Table 21**) (Ferguson et al., 2020).

Beyond supporting findings from the latent analysis, the individual gVRF-g mediation analysis of imaging features revealed that lower right and left ventricular volume for body size associates with greater vascular risk and lower cognitive function (**Figure 6, Supplementary Table 23**).

This result could point to a simple mechanistic step in the structural-functional hypothesis in which lower stroke volume for body size decreases cerebral perfusion (Rouch et al., 2022). Analysis of the individual brain features highlights grey matter, some subcortical volumes, and thalamic white matter tract measures as most mediating the gVRF-g association (**Figure 6, Supplementary Table 25**). This provides independent support from the joint analysis that these specific brain structures are key to the heart-brain axis.

Lower myocardial intensity has previously been associated with specific vascular risk factors and greater red meat consumption, and, here, we quantify its association with both greater aggregate vascular risk and lower cognitive function (Cetin et al., 2020; Raisi-Estabragh, Jaggi, et al., 2021; Raisi-Estabragh, McCracken, et al., 2021). Lower myocardial intensity strongly associates with higher vascular risk in a manner not explained by body or heart size (**Supplementary Table 15**). Additionally, myocardial thickness cannot explain the vascular risk - cognitive function association (**Supplementary Table 26**). These findings suggest that myocardial intensity is a myocardial size-independent biomarker for vascular risk. Lower myocardial intensity could have several biological interpretations. Previous imaging studies have detected myocardial fibrosis in cohorts of patients with vascular risk factors, suggesting that the low intensity features common to vascular risk and cognitive decline could be signs of a common myocardial fibrotic pathology driven by vascular risk factors (Mavrogeni et al., 2017; Ng et al., 2012; Turkbey et al., 2015). We also found some mediation via greater myocardial textural uniformity (**Supplementary Table 23**), which could also associate with the speculated fibrosis. Alternatively, since blood appears bright in CMR, lower myocardial intensity could suggest lower myocardial perfusion, compromising cardiac function and cerebral circulation. These results motivate further work to confirm these hypotheses through detailed imaging and tissue pathology.

Limitations

Although this study uses an exceptionally large dataset of adults across a wide range of middle- and older-ages, this work does not analyse longitudinal data. Therefore, we cannot disambiguate whether cardiovascular risk is causing decreased cognitive function, lower cognitive function is causing increased cardiovascular risk, or some mix of both effects. However, numerous

longitudinal studies in other cohorts support that cardiovascular risk associates with accelerated cognitive decline (Knopman et al., 2001; Rusanen et al., 2014; Samieri et al., 2018; SPRINT MIND Investigators for the SPRINT Research Group et al., 2019; W. Wang et al., 2022; Yaffe et al., 2014). Furthermore, without longitudinal imaging, we cannot assess the temporal relationship between cardiac and brain imaging phenotypes, vascular risk, and cognitive function. However, we argue that our results still offer novel cross-sectional support for the structural-functional model linking elevated vascular risk and poorer cognitive function.

In this work, we focus on the structural functional model linking vascular risk and cognitive function. Importantly, the VRF - CF association could be equally well explained by unmeasured mechanisms (e.g. metabolic hormonal dysregulation could directly impact neuronal function)(Benedict et al., 2007) or by reverse causation (e.g. poor cognitive function could decrease healthy lifestyle maintenance) (Batty et al., 2007; Calvin et al., 2011). Testing these hypotheses adequately would require longitudinal and biochemical data not yet available via the UK Biobank (Jensen et al., 2023; M. Wang et al., 2016). The UK Biobank does offer numerous measurements of possible confounders (socioeconomic status, geography, lifestyle, etc.) that could be used to rule out potential sources of error in our estimates. Although this study attempts to control for several well-studied sources of biometric and imaging confounding, future work could survey the wide array of possible confounders to refine our initial estimates.

We do not adjust for ethnicity in this study due to the low numbers of non-White British participants and the heterogeneity of those minority participants (**Supplementary Table 1**). Because the UK Biobank represents a relatively homogenous, well-educated, higher socioeconomic status, and predominantly Caucasian population, we emphasise the lack of generalizability of our findings to other populations. Neurovascular disease may differ significantly across populations of different ancestries and economies. Increased longitudinal biobanking of more diverse populations will be crucial to extending our findings to a more representative sample of the global population (Prictor et al., 2018; Ricard et al., 2023).

Whereas some have questioned the reliability of the UK Biobank cognitive exams (Lyall et al., 2016), recent work has supported their validity and psychometric properties (Fawns-Ritchie & Deary, 2020). Additionally, as reported in previous work, the effect sizes for the association between individual VRFs and cognitive exams is small, and we find no unique association for

many VRFs and at least two associations pointing in the ‘opposite direction’ as hypothesised (**Figure 5, Supplementary Tables 21**) (Lyall et al., 2017). Results from the full UK Biobank study suggest that large studies are needed to consistently detect these small effects and future increases to the imaging subset will help refine our results (Ferguson et al., 2020; Newby et al., 2021). We argue that the approach implemented here, via obtaining a latent measure g, minimises the impact of individual exam variability by obtaining an estimate of a robust, replicable, and test-invariant cognitive construct (Cox, Ritchie, et al., 2019; Fawns-Ritchie & Deary, 2020; Lyall et al., 2016).

Conclusion

The structural-functional model explaining the VRF-CF association rests on the argument that vascular risk drives changes in cardiovascular structure that lead to alterations in brain structure that lead to cognitive decline. Definitive support for the causal sequence of this model would require experimental or longitudinal work. However, our models (using cross-sectional data) are consistent with the hypothesis that vascular risk-associated cognitive ageing associates with distinctive variation in cardiac and brain structure. This is the first large-scale work to show that there is correlated variance in both heart and brain structure that mediates the association between vascular risk and cognitive function, providing a more extensive multi-modal framework to important prior work (Bai et al., 2020; Cox, Lyall, et al., 2019; Cox, Ritchie, et al., 2019; Ferguson et al., 2020; Lyall et al., 2017; McCracken et al., 2021; Newby et al., 2021; Raisi-Estabragh, Jaggi, et al., 2021; Raisi-Estabragh, M’Charrak, et al., 2021). One of the many hypotheses generated from analysing these data together is the identification of a key link to explain: how myocardial hypointensity could associate with cerebrovascular hypoperfusion impacting particular subcortical structures, like the thalamus.

Data and Code Availability

UK Biobank Data is available via application. All code open-sourced here: https://github.com/akshay-jaggi/heart_brain_mediation.

Contributions

	AJ	EC	ZRE	PG	CM	LZ	SN	SP	SC	KL
Funding Acquisition	X						X	X	X	X
Conceptualisation	X		X	X					X	X
Data Preprocessing	X		X	X	X	X				
Analysis and Coding	X	X								
Figure Development	X	X								
Writing	X									
Editing	X	X	X	X	X		X	X	X	X

Funding

AJ received funding from a Fulbright Pre-doctoral Research Award (2019–2020). This research was funded in whole, or in part, by the Wellcome Trust [221890/Z/20/Z and 108890/Z/15/Z]. For the purpose of open access, the author has applied a CC BY public copyright licence to any Author Accepted Manuscript version arising from this submission. ELSC is supported by funding from the Wellcome Trust 4-year PhD in Translational Neuroscience (108890/Z/15/Z).ZR-E recognises the National Institute for Health Research (NIHR) Integrated Academic Training programme which supports her Academic Clinical Lectureship post and was also supported by British Heart Foundation Clinical Research Training Fellowship No. FS/17/81/33318. Barts Charity (G-002346) contributed to fees required to access UK Biobank data [access application #2964]. SEP acknowledges the British Heart Foundation for funding the manual analysis to create a cardiovascular magnetic resonance imaging reference standard for

the UK Biobank imaging resource in 5000 CMR scans (www.bhf.org.uk; PG/14/89/31194). SEP acknowledges support from the National Institute for Health Research (NIHR) Biomedical Research Centre at Barts. PG, KL and SEP have received funding from the European Union's Horizon 2020 research and innovation programme under grant agreement No 825903 (euCanSHare project). SEP acknowledges support from and from the "SmartHeart" EPSRC programme grant (www.nihr.ac.uk; EP/P001009/1). SEP also acknowledges support from the CAP-AI programme, London's first AI enabling programme focused on stimulating growth in the capital's AI Sector. CAP-AI is led by Capital Enterprise in partnership with Barts Health NHS Trust and Digital Catapult and is funded by the European Regional Development Fund and Barts Charity. This article is supported by the London Medical Imaging and Artificial Intelligence Centre for Value Based Healthcare (AI4VBH), which is funded from the Data to Early Diagnosis and Precision Medicine strand of the government's Industrial Strategy Challenge Fund, managed and delivered by Innovate UK on behalf of UK Research and Innovation (UKRI). Views expressed are those of the authors and not necessarily those of the AI4VBH Consortium members, the NHS, Innovate UK, or UKRI. This work was supported by Health Data Research UK, an initiative funded by UK Research and Innovation, Department of Health and Social Care (England) and the devolved administrations, and leading medical research charities. This project was enabled through access to the MRC eMedLab Medical Bioinformatics infrastructure, supported by the Medical Research Council (www.mrc.ac.uk; MR/L016311/1). SRC is supported by a Sir Henry Dale Fellowship, jointly funded by the Wellcome Trust and the Royal Society (221890/Z/20/Z), and acknowledges funding from Biotechnology and Biological Sciences Research Council, and the Economic and Social Research Council (BB/W008793/1), Age UK (The Disconnected Mind project), the US National Institutes of Health (R01AG054628; 1RF1AG073593), the Medical Research Council (MR/R024065/1), and The University of Edinburgh. KL received funding from the Spanish Ministry of Science, Innovation and Universities under grant agreement RTI2018-099898-B-I00.

Declaration of Competing Interests

SEP provides Consultancy to Circle Cardiovascular Imaging, Inc., Calgary, Alberta, Canada.

Ethics

UK Biobank has ethics approval from the North West Multi-centre Research Ethics Committee as a Research Tissue Bank approval.

Acknowledgments

We thank the UK Biobank participants and the UK Biobank team for their work in collecting, processing and disseminating data for analysis. We thank Victor Campello, Carlos Martín-Isla, Cristian Izquierdo Morcillo, Mika Sarkin Jain, Vaibhav Mohanty, Anna Sappington, and Ralph Ignacio Lawton for helpful discussions and scientific feedback. The authors also thank Katharina F Heil and Clara Badimon for administrative support.

References

Alfaro-Almagro, F., Jenkinson, M., Bangerter, N. K., Andersson, J. L. R., Griffanti, L., Douaud, G., Sotiropoulos, S. N., Jbabdi, S., Hernandez-Fernandez, M., Vallee, E., Vidaurre, D., Webster, M., McCarthy, P., Rorden, C., Daducci, A., Alexander, D. C., Zhang, H., Dragonu, I., Matthews, P. M., … Smith, S. M. (2018). Image processing and Quality Control for the first 10,000 brain imaging datasets from UK Biobank. *NeuroImage*, *166*, 400–424.

Alfaro-Almagro, F., McCarthy, P., Afyouni, S., Andersson, J. L. R., Bastiani, M., Miller, K. L., Nichols, T. E., & Smith, S. M. (2021). Confound modelling in UK Biobank brain imaging. *NeuroImage*, *224*, 117002.

Antonopoulos, A. S., Boutsikou, M., Simantiris, S., Angelopoulos, A., Lazaros, G., Panagiotopoulos, I., Oikonomou, E., Kanoupaki, M., Tousoulis, D., Mohiaddin, R. H., Tsioufis, K., & Vlachopoulos, C. (2021). Machine learning of native T1 mapping radiomics for classification of hypertrophic cardiomyopathy phenotypes. *Scientific Reports*, *11*(1), 23596.

Bai, W., Suzuki, H., Huang, J., Francis, C., Wang, S., Tarroni, G., Guitton, F., Aung, N., Fung, K., Petersen, S. E., Piechnik, S. K., Neubauer, S., Evangelou, E., Dehghan, A., O'Regan, D. P., Wilkins, M. R., Guo, Y., Matthews, P. M., & Rueckert, D. (2020). A population-based phenome-wide association study of cardiac and aortic structure and function. *Nature Medicine*, *26*(10), 1654–1662.

Banus, J., Lorenzi, M., Camara, O., & Sermesant, M. (2021). Biophysics-based statistical learning: Application to heart and brain interactions. *Medical Image Analysis*, *72*, 102089.

Batty, G. D., Deary, I. J., & Gottfredson, L. S. (2007). Premorbid (early life) IQ and later mortality risk: systematic review. *Annals of Epidemiology*, *17*(4), 278–288.

Benedict, C., Hallschmid, M., Schmitz, K., Schultes, B., Ratter, F., Fehm, H. L., Born, J., & Kern, W. (2007). Intranasal insulin improves memory in humans: superiority of insulin aspart. *Neuropsychopharmacology: Official Publication of the American College of Neuropsychopharmacology*, *32*(1), 239–243.

Bohlken, M. M., Brouwer, R. M., Mandl, R. C. W., van Haren, N. E. M., Brans, R. G. H., van Baal, G. C. M., de Geus, E. J. C., Boomsma, D. I., Kahn, R. S., & Hulshoff Pol, H. E. (2014). Genes contributing to subcortical volumes and intellectual ability implicate the thalamus. *Human Brain Mapping*, *35*(6), 2632–2642.

Calvin, C. M., Deary, I. J., Fenton, C., Roberts, B. A., Der, G., Leckenby, N., & Batty, G. D. (2011). Intelligence in youth and all-cause-mortality: systematic review with meta-analysis. *International Journal of Epidemiology*, *40*(3), 626–644.

Cetin, I., Raisi-Estabragh, Z., Petersen, S. E., Napel, S., Piechnik, S. K., Neubauer, S., Gonzalez Ballester, M. A., Camara, O., & Lekadir, K. (2020). Radiomics Signatures of Cardiovascular Risk Factors in Cardiac MRI: Results From the UK Biobank. *Frontiers in Cardiovascular Medicine*, *7*, 591368.

Cox, S. R., Lyall, D. M., Ritchie, S. J., Bastin, M. E., Harris, M. A., Buchanan, C. R., Fawns-Ritchie, C., Barbu, M. C., de Nooij, L., Reus, L. M., Alloza, C., Shen, X., Neilson, E., Alderson, H. L., Hunter, S., Liewald, D. C., Whalley, H. C., McIntosh, A. M., Lawrie, S. M., … Deary, I. J. (2019). Associations between vascular risk factors and brain MRI indices in UK Biobank. *European Heart Journal*, *40*(28), 2290–2300.

Cox, S. R., Ritchie, S. J., Fawns-Ritchie, C., Tucker-Drob, E. M., & Deary, I. J. (2019). Structural brain imaging correlates of general intelligence in UK Biobank. *Intelligence*, *76*, 101376.

Cox, S. R., Ritchie, S. J., Tucker-Drob, E. M., Liewald, D. C., Hagenaars, S. P., Davies, G., Wardlaw, J. M., Gale, C. R., Bastin, M. E., & Deary, I. J. (2016). Ageing and brain white matter structure in 3,513 UK Biobank participants. *Nature Communications*, *7*, 13629.

Deary, I. J., Penke, L., & Johnson, W. (2010). The neuroscience of human intelligence differences. *Nature Reviews. Neuroscience*, *11*(3), 201–211.

de la Torre, J. C. (2012a). Cardiovascular risk factors promote brain hypoperfusion leading to cognitive decline and dementia. *Cardiovascular Psychiatry and Neurology*, *2012*, 367516.

de la Torre, J. C. (2012b). Cerebral hemodynamics and vascular risk factors: setting the stage for

Alzheimer's disease. *Journal of Alzheimer's Disease: JAD*, *32*(3), 553–567.

Elliott, L. T., Sharp, K., Alfaro-Almagro, F., Shi, S., Miller, K. L., Douaud, G., Marchini, J., & Smith, S. M. (2018). Genome-wide association studies of brain imaging phenotypes in UK Biobank. *Nature*, *562*(7726), 210–216.

Fawns-Ritchie, C., & Deary, I. J. (2020). Reliability and validity of the UK Biobank cognitive tests. *PloS One*, *15*(4), e0231627.

Ferguson, A. C., Tank, R., Lyall, L. M., Ward, J., Welsh, P., Celis-Morales, C., McQueenie, R., Strawbridge, R. J., Mackay, D. F., Pell, J. P., Smith, D. J., Sattar, N., Cavanagh, J., & Lyall, D. M. (2020). Association of SBP and BMI with cognitive and structural brain phenotypes in UK Biobank. *Journal of Hypertension*, *38*(12), 2482–2489.

Gorelick, P. B., Furie, K. L., Iadecola, C., Smith, E. E., Waddy, S. P., Lloyd-Jones, D. M., Bae, H.-J., Bauman, M. A., Dichgans, M., Duncan, P. W., Girgus, M., Howard, V. J., Lazar, R. M., Seshadri, S., Testai, F. D., van Gaal, S., Yaffe, K., Wasiak, H., Zerna, C., & American Heart Association/American Stroke Association. (2017). Defining Optimal Brain Health in Adults: A Presidential Advisory From the American Heart Association/American Stroke Association. *Stroke; a Journal of Cerebral Circulation*, *48*(10), e284–e303.

Gorelick, P. B., Scuteri, A., Black, S. E., Decarli, C., Greenberg, S. M., Iadecola, C., Launer, L. J., Laurent, S., Lopez, O. L., Nyenhuis, D., Petersen, R. C., Schneider, J. A., Tzourio, C., Arnett, D. K., Bennett, D. A., Chui, H. C., Higashida, R. T., Lindquist, R., Nilsson, P. M., … American Heart Association Stroke Council, Council on Epidemiology and Prevention, Council on Cardiovascular Nursing, Council on Cardiovascular Radiology and Intervention, and Council on Cardiovascular Surgery and Anesthesia. (2011). Vascular contributions to cognitive impairment and dementia: a statement for healthcare professionals from the american heart association/american stroke association. *Stroke; a Journal of Cerebral Circulation*, *42*(9), 2672–2713.

Gorelick, P. B., & Sorond, F. (2018). Vascular risk burden, brain health, and next steps [Review of *Vascular risk burden, brain health, and next steps*]. *Neurology*, *91*(16), 729–730. AAN Enterprises.

Haley, A. P., Oleson, S., Pasha, E., Birdsill, A., Kaur, S., Thompson, J., & Tanaka, H. (2018). Phenotypic heterogeneity of obesity-related brain vulnerability: one-size interventions will not fit all. *Annals of the New York Academy of Sciences*, *1428*(1), 89–102.

Hamer, M., & Batty, G. D. (2019). Association of body mass index and waist-to-hip ratio with brain structure: UK Biobank study. *Neurology*, *92*(6), e594–e600.

Iadecola, C., Yaffe, K., Biller, J., Bratzke, L. C., Faraci, F. M., Gorelick, P. B., Gulati, M., Kamel, H., Knopman, D. S., Launer, L. J., Saczynski, J. S., Seshadri, S., Zeki Al Hazzouri, A., & American Heart Association Council on Hypertension; Council on Clinical Cardiology; Council on Cardiovascular Disease in the Young; Council on Cardiovascular and Stroke Nursing; Council on Quality of Care and Outcomes Research; and Stroke Council. (2016). Impact of Hypertension on Cognitive Function: A Scientific Statement From the American Heart Association. *Hypertension*, *68*(6), e67–e94.

Jefferson, A. L., Himali, J. J., Beiser, A. S., Au, R., Massaro, J. M., Seshadri, S., Gona, P., Salton, C. J., DeCarli, C., O'Donnell, C. J., Benjamin, E. J., Wolf, P. A., & Manning, W. J. (2010). Cardiac index is associated with brain aging: the Framingham Heart Study. *Circulation*, *122*(7), 690–697.

Jensen, M., Zeller, T., Twerenbold, R., & Thomalla, G. (2023). Circulating cardiac biomarkers, structural brain changes, and dementia: Emerging insights and perspectives. *Alzheimer's & Dementia: The Journal of the Alzheimer's Association*, *19*(4), 1529–1548.

John, L. K., Loewenstein, G., & Prelec, D. (2012). Measuring the prevalence of questionable research practices with incentives for truth telling. *Psychological Science*, *23*(5), 524–532.

Knopman, D., Boland, L. L., Mosley, T., Howard, G., Liao, D., Szklo, M., McGovern, P., Folsom, A. R., & Atherosclerosis Risk in Communities (ARIC) Study Investigators. (2001). Cardiovascular risk factors and cognitive decline in middle-aged adults. *Neurology*, *56*(1), 42–48.

Liang, Y., Melia, O., Caroll, T. J., Brettin, T., Brown, A., & Im, H. K. (2021). BrainXcan identifies brain features associated with behavioral and psychiatric traits using large scale genetic and imaging data. In *bioRxiv*. medRxiv. https://doi.org/10.1101/2021.06.01.21258159

Lyall, D. M., Celis-Morales, C. A., Anderson, J., Gill, J. M. R., Mackay, D. F., McIntosh, A. M., Smith, D. J., Deary, I. J., Sattar, N., & Pell, J. P. (2017). Associations between single and multiple cardiometabolic diseases and cognitive abilities in 474 129 UK Biobank participants. *European Heart Journal*, *38*(8), 577–583.

Lyall, D. M., Cullen, B., Allerhand, M., Smith, D. J., Mackay, D., Evans, J., Anderson, J., Fawns-Ritchie, C., McIntosh, A. M., Deary, I. J., & Pell, J. P. (2016). Cognitive Test Scores in UK Biobank: Data Reduction in 480,416 Participants and Longitudinal Stability in 20,346 Participants. *PloS One*, *11*(4), e0154222.

Mavrogeni, S., Katsi, V., Vartela, V., Noutsias, M., Markousis-Mavrogenis, G., Kolovou, G., & Manolis, A. (2017). The emerging role of Cardiovascular Magnetic Resonance in the evaluation of hypertensive heart disease. *BMC Cardiovascular Disorders*, *17*(1), 132.

McCormick, E. M., Borgeest, G. S., & Kievit, R. (2022). *Interrupted mediation: A cautionary note on using derived metrics as intervening variables in path models*. https://doi.org/10.31234/osf.io/48xj5

McCracken, C., Raisi-Estabragh, Z., Raman, B., Dennis, A., Nichols, T. E., Husain, M., Petersen, S. E., & Neubauer, S. (2021). 6 Healthier CMR phenotypes are linked to favourable brain MRI structure and function metrics in the UK Biobank. *Heart* , *107*(Suppl 3), A4–A5.

McCracken, C., Raisi-Estabragh, Z., Veldsman, M., Raman, B., Dennis, A., Husain, M., Nichols, T. E., Petersen, S. E., & Neubauer, S. (2022). Multi-organ imaging demonstrates the heart-brain-liver axis in UK Biobank participants. *Nature Communications*, *13*(1), 7839.

Miller, K. L., Alfaro-Almagro, F., Bangerter, N. K., Thomas, D. L., Yacoub, E., Xu, J., Bartsch, A. J., Jbabdi, S., Sotiropoulos, S. N., Andersson, J. L. R., Griffanti, L., Douaud, G., Okell, T. W., Weale, P., Dragonu, I., Garratt, S., Hudson, S., Collins, R., Jenkinson, M., … Smith, S. M. (2016). Multimodal population brain imaging in the UK Biobank prospective epidemiological study. *Nature Neuroscience*, *19*(11), 1523–1536.

Newby, D., Winchester, L., Sproviero, W., Fernandes, M., Wang, D., Kormilitzin, A., Launer, L. J., & Nevado-Holgado, A. J. (2021). Associations Between Brain Volumes and Cognitive Tests with

Hypertensive Burden in UK Biobank. *Journal of Alzheimer's Disease: JAD*, *84*(3), 1373–1389.

Ng, A. C. T., Auger, D., Delgado, V., van Elderen, S. G. C., Bertini, M., Siebelink, H.-M., van der Geest, R. J., Bonetti, C., van der Velde, E. T., de Roos, A., Smit, J. W. A., Leung, D. Y., Bax, J. J., & Lamb, H. J. (2012). Association between diffuse myocardial fibrosis by cardiac magnetic resonance contrast-enhanced T_1 mapping and subclinical myocardial dysfunction in diabetic patients: a pilot study. *Circulation. Cardiovascular Imaging*, *5*(1), 51–59.

Pasha, E. P., Birdsill, A. C., Oleson, S., Haley, A. P., & Tanaka, H. (2017). Impacts of Metabolic Syndrome Scores on Cerebrovascular Conductance Are Mediated by Arterial Stiffening. *American Journal of Hypertension*, *31*(1), 72–79.

Payabvash, S., Souza, L. C. S., Wang, Y., Schaefer, P. W., Furie, K. L., Halpern, E. F., Gonzalez, R. G., & Lev, M. H. (2011). Regional ischemic vulnerability of the brain to hypoperfusion: the need for location specific computed tomography perfusion thresholds in acute stroke patients. *Stroke; a Journal of Cerebral Circulation*, *42*(5), 1255–1260.

Prictor, M., Teare, H. J. A., & Kaye, J. (2018). Equitable Participation in Biobanks: The Risks and Benefits of a "Dynamic Consent" Approach. *Frontiers in Public Health*, *6*, 253.

Qiu, C., & Fratiglioni, L. (2015). A major role for cardiovascular burden in age-related cognitive decline. *Nature Reviews. Cardiology*, *12*(5), 267–277.

Raisi-Estabragh, Z., Izquierdo, C., Campello, V. M., Martin-Isla, C., Jaggi, A., Harvey, N. C., Lekadir, K., & Petersen, S. E. (2020). Cardiac magnetic resonance radiomics: basic principles and clinical perspectives. *European Heart Journal Cardiovascular Imaging*, *21*(4), 349–356.

Raisi-Estabragh, Z., Jaggi, A., Gkontra, P., Mccracken, C., Aung, N., Munroe, P. B., Neubauer, S., Harvey, N. C., Lekadir, K., & Petersen, S. E. (2021). Cardiac magnetic resonance radiomics reveal differential impact of sex, age, and vascular risk factors on cardiac structure and myocardial tissue. *Frontiers in Cardiovascular Medicine*, *8*, 1972.

Raisi-Estabragh, Z., McCracken, C., Gkontra, P., Jaggi, A., Ardissino, M., Cooper, J., Biasiolli, L., Aung, N., Piechnik, S. K., Neubauer, S., Munroe, P. B., Lekadir, K., Harvey, N. C., & Petersen, S. E.

(2021). Associations of Meat and Fish Consumption With Conventional and Radiomics Cardiovascular Magnetic Resonance Phenotypes in the UK Biobank. *Frontiers in Cardiovascular Medicine*, *8*, 667849.

Raisi-Estabragh, Z., M'Charrak, A., McCracken, C., Biasiolli, L., Ardissino, M., Curtis, E. M., Aung, N., Suemoto, C. K., Mackay, C., Suri, S., Nichols, T. E., Harvey, N. C., Petersen, S. E., & Neubauer, S. (2021). Associations of cognitive performance with cardiovascular magnetic resonance phenotypes in the UK Biobank. *European Heart Journal Cardiovascular Imaging*. https://doi.org/10.1093/ehjci/jeab075

Ricard, J. A., Parker, T. C., Dhamala, E., Kwasa, J., Allsop, A., & Holmes, A. J. (2023). Confronting racially exclusionary practices in the acquisition and analyses of neuroimaging data. *Nature Neuroscience*, *26*(1), 4–11.

Rikhye, R. V., Wimmer, R. D., & Halassa, M. M. (2018). Toward an Integrative Theory of Thalamic Function. *Annual Review of Neuroscience*, *41*, 163–183.

Rouch, L., Hoang, T., Xia, F., Sidney, S., Lima, J. A. C., & Yaffe, K. (2022). Twenty-Five-Year Change in Cardiac Structure and Function and Midlife Cognition: The CARDIA Study. *Neurology*, *98*(10), e1040–e1049.

Rusanen, M., Kivipelto, M., Levälahti, E., Laatikainen, T., Tuomilehto, J., Soininen, H., & Ngandu, T. (2014). Heart diseases and long-term risk of dementia and Alzheimer's disease: a population-based CAIDE study. *Journal of Alzheimer's Disease: JAD*, *42*(1), 183–191.

Samieri, C., Perier, M.-C., Gaye, B., Proust-Lima, C., Helmer, C., Dartigues, J.-F., Berr, C., Tzourio, C., & Empana, J.-P. (2018). Association of Cardiovascular Health Level in Older Age With Cognitive Decline and Incident Dementia. *JAMA: The Journal of the American Medical Association*, *320*(7), 657–664.

Shen, J., Tozer, D. J., Markus, H. S., & Tay, J. (2020). Network efficiency mediates the relationship between vascular burden and cognitive impairment: A diffusion tensor imaging study in UK Biobank. *Stroke; a Journal of Cerebral Circulation*, *51*(6), 1682–1689.

SPRINT MIND Investigators for the SPRINT Research Group, Williamson, J. D., Pajewski, N. M., Auchus, A. P., Bryan, R. N., Chelune, G., Cheung, A. K., Cleveland, M. L., Coker, L. H., Crowe, M. G., Cushman, W. C., Cutler, J. A., Davatzikos, C., Desiderio, L., Erus, G., Fine, L. J., Gaussoin, S. A., Harris, D., Hsieh, M.-K., … Wright, C. B. (2019). Effect of Intensive vs Standard Blood Pressure Control on Probable Dementia: A Randomized Clinical Trial. *JAMA: The Journal of the American Medical Association*, *321*(6), 553–561.

Sweeney, M. D., Kisler, K., Montagne, A., Toga, A. W., & Zlokovic, B. V. (2018). The role of brain vasculature in neurodegenerative disorders. *Nature Neuroscience*, *21*(10), 1318–1331.

Truhn, D., Schrading, S., Haarburger, C., Schneider, H., Merhof, D., & Kuhl, C. (2019). Radiomic versus Convolutional Neural Networks Analysis for Classification of Contrast-enhancing Lesions at Multiparametric Breast MRI. *Radiology*, *290*(2), 290–297.

Turkbey, E. B., Nacif, M. S., Guo, M., McClelland, R. L., Teixeira, P. B. R. P., Bild, D. E., Barr, R. G., Shea, S., Post, W., Burke, G., Budoff, M. J., Folsom, A. R., Liu, C.-Y., Lima, J. A., & Bluemke, D. A. (2015). Prevalence and Correlates of Myocardial Scar in a US Cohort. *JAMA: The Journal of the American Medical Association*, *314*(18), 1945–1954.

Ukbb-Prot-, P. N. (n.d.). *UK Biobank: Protocol for a large-scale prospective epidemiological resource*. https://www.ukbiobank.ac.uk/media/gnkeyh2q/study-rationale.pdf

van Buchem, M. A., Biessels, G. J., Brunner la Rocca, H. P., de Craen, A. J. M., van der Flier, W. M., Ikram, M. A., Kappelle, L. J., Koudstaal, P. J., Mooijaart, S. P., Niessen, W., van Oostenbrugge, R., de Roos, A., van Rossum, A. C., & Daemen, M. J. A. P. (2014). The heart-brain connection: a multidisciplinary approach targeting a missing link in the pathophysiology of vascular cognitive impairment. *Journal of Alzheimer's Disease: JAD*, *42 Suppl 4*, S443–S451.

van Griethuysen, J. J. M., Fedorov, A., Parmar, C., Hosny, A., Aucoin, N., Narayan, V., Beets-Tan, R. G. H., Fillion-Robin, J.-C., Pieper, S., & Aerts, H. J. W. L. (2017). Computational Radiomics System to Decode the Radiographic Phenotype. *Cancer Research*, *77*(21), e104–e107.

Wang, M., Norman, J. E., Srinivasan, V. J., & Rutledge, J. C. (2016). Metabolic, inflammatory, and

microvascular determinants of white matter disease and cognitive decline. *American Journal of Neurodegenerative Disease*, *5*(5), 171–177.

Wang, W., Zhang, M. J., Inciardi, R. M., Norby, F. L., Johansen, M. C., Parikh, R., Van't Hof, J. R., Alonso, A., Soliman, E. Z., Mosley, T. H., Gottesman, R. F., Shah, A. M., Solomon, S. D., & Chen, L. Y. (2022). Association of Echocardiographic Measures of Left Atrial Function and Size With Incident Dementia. *JAMA: The Journal of the American Medical Association*, *327*(12), 1138–1148.

Wardlaw, J. M., Allerhand, M., Doubal, F. N., Valdes Hernandez, M., Morris, Z., Gow, A. J., Bastin, M., Starr, J. M., Dennis, M. S., & Deary, I. J. (2014). Vascular risk factors, large-artery atheroma, and brain white matter hyperintensities. *Neurology*, *82*(15), 1331–1338.

Wimo, A., Jönsson, L., Bond, J., Prince, M., Winblad, B., & Alzheimer Disease International. (2013). The worldwide economic impact of dementia 2010. *Alzheimer's & Dementia: The Journal of the Alzheimer's Association*, *9*(1), 1–11.e3.

Yaffe, K., Vittinghoff, E., Pletcher, M. J., Hoang, T. D., Launer, L. J., Whitmer, R., Coker, L. H., & Sidney, S. (2014). Early adult to midlife cardiovascular risk factors and cognitive function. *Circulation*, *129*(15), 1560–1567.

Zenger, B., Rizzi, S., Steinberg, B. A., Ranjan, R., & Bunch, T. J. (2023). This is Your Brain, and This is Your Brain on Atrial Fibrillation: The Roles of Cardiac Malperfusion Events and Vascular Dysfunction in Cognitive Impairment. *Arrhythmia & Electrophysiology Review*, *12*, e01.

Zhang, Y., Oikonomou, A., Wong, A., Haider, M. A., & Khalvati, F. (2017). Radiomics-based Prognosis Analysis for Non-Small Cell Lung Cancer. *Scientific Reports*, *7*, 46349.

Zhao, B., Li, T., Fan, Z., Yang, Y., Shu, J., Yang, X., Wang, X., Luo, T., Tang, J., Xiong, D., Wu, Z., Li, B., Chen, J., Shan, Y., Tomlinson, C., Zhu, Z., Li, Y., Stein, J. L., & Zhu, H. (2023). Heart-brain connections: Phenotypic and genetic insights from magnetic resonance images. *Science*, *380*(6648), abn6598.

Supplementary Methods

Acquisition and Processing

Vascular Risk Factors

Diabetes diagnosis was confirmed by combining data from 'Diagnosed by doctor,' self-report, ICD10 codes, first HES recorded occurrences, recorded use of insulin, and blood glycated haemoglobin levels (HbA1c). Hypercholesterolemia was confirmed by combining data from ICD10 codes, first HES recorded occurrences, recorded use of cholesterol lowering agents, and blood cholesterol levels. Hypertension was confirmed by combining data from self-report, ICD10 codes, first HES recorded occurrences, recorded use of blood pressure medications, and an HES physician diagnosis of hypertension. In all cases, if one or more of these measures was consistent with the diagnosis, we considered the individual as having the diagnosis. Exact list of UK Biobank field IDs found in prior publication (Raisi-Estabragh, Jaggi, et al., 2021).

Cardiac Imaging

The UK Biobank acquired all images according to predefined standardised operating procedures (Petersen et al., 2016; Raisi-Estabragh, Harvey, et al., 2021). The relevant imaging comprised of a complete short axis stack covering the left and right ventricles acquired at one slice per breath hold using balanced steady- state free precession (bSSFP) sequences. Typical acquisition parameters are as follows: TR/TE = 2.6.1.1 ms, flip angle 80 degrees, Grappa factor 2, voxel size 1.8mm × 1.8mm × 8mm. The actual temporal resolution of 32ms was interpolated to 50 phases per cardiac cycle (~20 ms). With the exception of distortion correction, no signal or image filtering was applied.

The first 5,000 UK Biobank CMR scans were manually segmented using CVI42 post-processing software (Version 5.1.1, Circle Cardiovascular Imaging Inc., Calgary, Canada). The analysis protocol has been previously published.

In brief, LV endocardial and epicardial borders were contoured in end-diastole and end-systole in the short axis stack images. End-diastole was defined as the first phase of the acquisition. End-systole was selected as the cardiac phase at which the mid-ventricular LV intra-cavity blood pool appeared smallest by visual inspection. The right ventricular (RV) endocardial borders were segmented in end-diastole and end-systole. This manual ground-truth dataset was used to develop a fully automated image segmentation algorithm applied to the rest of the available UK Biobank CMR studies (Attar et al., 2019; Bai et al., 2018; Petersen et al., 2017).

The segmentations from the short axis stack were then used to define three regions of interest for radiomics analysis: RV cavity, LV cavity, LV myocardium. Radiomics features are calculated from 3D volumes of these ROIs. On a high level, the shape features capture volume, maximal diameter, elongation, and related features of each structure; the intensity features capture global intensity statistics like mean MR intensity of each structure; and the texture features capture local patterns of MR intensity using methods like grey-level co-occurrence matrices. To reduce intensity level variations attributable to the acquisition process, we performed intensity normalisation of images through histogram matching, using as reference one of the studies from the dataset (Carré et al., 2020; van Timmeren et al., 2020). For grey level discretisation, we used a fixed bin width of 25 intensity values. Along with radiomics features, we also extracted traditional measures, including left ventricular end-systolic volume (LVESV), end-diastolic volume (LVEDV), stroke volume (LVSV), ejection fraction (LVEF), corresponding right-ventricular values (RVESV, RVEDV, RVSV, RVEF), and left ventricular mass (LVM).

Lastly, in a subset of our cohort consisting of 7118 individuals, we computed 78 features as prescribed in Bai, et al. (Bai et al., 2020). Specifically, we generated wall thickness features from short axis images, including global mean wall thickness and the mean wall thickness of 16 American Heart Association (AHA) segments (denoted as WT_AHA_1, …, WT_AHA_16). From long axis images, we generated LA maximum volume (LAV.max), LA minimum volume (LAV.min), LA stroke volume (LASV), LA ejection fraction (LAEF), RA maximum volume (RAV.max), RA minimum volume (RAV.min), RV stroke volume (RASV), and RA ejection fraction (RAEF). From aortic cine image features, we included AAo maximum area, AAo minimum area, AAo distensibility, DAo maximum area, DAo minimum area, and DAo distensibility. We computed circumferential and radial strains (Ecc and Err) globally and from

the 16 AHA segments. Lastly, we compute peak longitudinal strains (Ell) globally and from six segments of the myocardial contour based on the long axis images: basal septal, basal lateral, mid septal, mid lateral, apical septal, and apical lateral.

Brain Imaging

All brain MRI data were acquired on the same model of 3T Siemens Skyra scanner, according to a freely available protocol (Alfaro-Almagro et al., 2018). All imaging parameters have been reported previously (Cox, Lyall, et al., 2019; Cox, Ritchie, et al., 2019). T1-weighted MPRAGE and T2-weighted FLAIR volumes were acquired in sagittal orientation at 1 × 1 × 1 mm and 1.05 × 1 × 1 mm resolution, respectively. The dMRI acquisition comprised a spin-echo echo-planar sequence with 10 T2-weighted ($b \approx 0$ s mm^{-2}) baseline volumes, 50 $b = 1000$ s mm^{-2} and 50 $b = 2000$ s mm^{-2} diffusion weighted volumes, with 100 distinct diffusion-encoding directions and 2 mm isotropic voxels.

The IDPs in this study included total brain volume, grey matter volume, subcortical volumes (accumbens, amygdala, caudate, hippocampus, pallidum, putamen, thalamus), and tract-averaged fractional anisotropy (FA), mean diffusivity (MD), intra-cellular volume fraction (ICVF), isotropic or free water volume fraction (ISOVF), orientation dispersion index (OD), diffusion principal axis strengths (L1-3), and diffusion tensor mode (MO) of the following white matter tracts: acoustic radiation, anterior thalamic, cingulum gyrus, and parahippocampal, corticospinal, forceps major and minor, inferior fronto-occipital, inferior longitudinal, middle cerebellar peduncle, medial lemniscus, posterior thalamic, superior longitudinal, superior thalamic, and uncinate.

Analysis

Workflow

Heart Disease Filtering

To filter out patients with severe cardiovascular pathology, we identified all patients with any ischaemic heart disease, non-ischaemic cardiomyopathy, valvular disease, or significant

arrhythmia. We derived these diagnoses through a combination of self-reported answers at baseline interview, UK Biobank algorithmically-computed outcomes, and linked HES data codes, reported in detail previously (Raisi-Estabragh, Jaggi, et al., 2021). 1311 of the 13709 subjects that passed initial filtering for completeness had at least one of the above conditions.

Brain Disease Filtering

To align with previous studies and observe only non-pathological variation in cognitive function and brain structure (Cox, Lyall, et al., 2019), we removed all patients with the following diseases provided via self-report during the baseline UK Biobank session: dementia, parkinsons, other chronic/ neurodegenerative, Guillain-Barré, multiple sclerosis, other demyelinating, stroke, brain haemorrhage, brain/intracranial abscess, cerebral aneurysm, cerebral palsy, encephalitis, epilepsy, head injury, infection of nervous system, ischaemic stroke, meningioma (benign), meningitis, motor neuron disease, neurological injury/trauma, spina bifida, subdural haematoma, subarachnoid haemorrhage, transient ischaemic attack, brain cancer, and meningeal cancer. 524 of the 13709 subjects that passed initial filtering for completeness had at least one of the above conditions.

Dimensionality Reduction

CMR Radiomics PCA

To select the number of robust principal components to retain for downstream analysis, we ran 10-fold cross validation over the dataset, computed principal components on the training data, computed the explained variance in the held-out data, plotted the explained variance, and found the elbow in this curve, the point after which the explained variance stops decreasing across PCs.

Here we offer interpretations of the loadings of the principal components to understand their significance (**Supplementary Table 4**). The first PC has large weights for myocardial volume, surface area, and several global texture features correlated with myocardial size. The second PC has large weights for measures of the centre of the myocardial voxel intensity distribution (e.g. mean, median) with end-systolic intensities having higher weights relative to end-diastolic. The third PC has large negative weights for measures of the variability of the myocardial textures

(e.g. entropy, contrast). Such that the value of the third PC correlates with complexity, we used the negative of its PC scores.

Brain MRI IDP PCA Interpretation

For the Factor Analysis, tract measures (left and right) were entered separately into this analysis, correlated residuals between the left and right of each tract and between some other tracts were allowed.

We offer interpretations of the loadings of the first three unrotated principal components of the Brain MRI IDPs (**Supplementary Table 6**). The first PC has high weightings for ICVF and FA of the fasciculi and thalamic tracts. In previous literature, low FA and high MD have been associated with greater age, elevated vascular risk, and lower processing speed (Cox et al., 2016; Cox, Lyall, et al., 2019; Penke et al., 2010). The second PC has large negative weightings for FA of the corticospinal tracts. We took the negative of the second PC scores such that the second PC increases with greater FA. The third has high weightings for volumes, suggesting a factor capturing size.

Heart-Brain Joint Factor Interpretation

To choose the number of CCA modes to keep, we performed 10-fold cross validation on the subjects. For each training fold, we computed ten CCA modes and extracted their loadings. We then applied the loadings to the held-out testing data and found the correlation of the heart and brain components in the held-out data. We then plotted the correlation and chose the number of modes to the left of the elbow, or before the correlation in the modes levels off. Like the PCA method, this cross-validation method ensures that we choose a number of features with reasonable explained variance in unseen UK Biobank subjects.

To assess what features are most important to each mode, we found the correlation of the component scores with the features of each dataset (**Supplementary Table 7**). We found that most interesting associations were negative for the first two modes, so we inverted the sign of their component scores for clarity. The scores of the first mode correlate with most volume measures from both the heart and brain imaging. The scores of the second mode correlate with myocardial intensity in end-systole and correlate with some measures of volume of the brain

image (notably grey matter volume) and many measures of white matter integrity (ICVF and FA) in the thalamic tracts. This mode also has a strong negative correlation with white matter hyperintensity volume. We expect both volumes to decrease and FA to decrease in neurovascular pathology, so this mode likely correlates with neurovascular health (Cox, Lyall, et al., 2019). The scores of the third mode correlate with myocardial intensity in end-diastole, and they also correlate with MD.

Imaging Deconfounding

Both of the imaging datasets generate features sensitive to the size of patients and their position in the scanner. To remove potential confounding on downstream analyses, we regressed all latent variables for the imaging datasets on the imaging confounders and performed future analyses on the residuals of this regression. For the cardiac imaging latents, we regressed each latent onto z-scored body surface area (BSA). We regressed each brain imaging latent onto z-scored head size and the head position in the scanner (X, Y, and Z coordinates). We regressed the components of the joint factors on both the heart and brain imaging confounders because the joint analysis can induce correlations with imaging conditions from either dataset. In analyses that use individual imaging features, we perform this deconfounding on individual features rather than the latent features. Since the uncorrected values may be of interest in some contexts, we report both the uncorrected and corrected values for all analyses in the **Supplementary Tables**.

Linear Models

In **Figure 3, Supplementary Tables 9, 10**, we report the results of linearly modelling each latent measure as a function of each other latent measure controlling for sex and age. We report additional R^2 as the amount of variance that the independent latent measure explains in the dependent latent measure above what is already explained by the covariates.

Mediation Modelling

Since mediation modelling has been described in detail elsewhere (MacKinnon et al., 2007), we will provide a brief explanation of the procedure in the context of this study. We first regress a potential mediator, say grey matter, on gVRF. Label this coefficient $\boldsymbol{a}$. We then regress g on both

the mediator and gVRF. The coefficient for the mediator is ***b***, and the coefficient for gVRF is ***c'***. The indirect effect of gVRF on g via the mediator is ***a*b***, and the direct effect of VRF on g is ***c'***. The magnitude of the indirect effect indicates the degree to which a mediator explains the observed association between gVRF and g. The total effect is ***c=c'+a*b***. The percent mediation is the ratio of the indirect effect and the total effect: ***a*b/(c'+a*b)***.

Along with single mediation, we also performed and report parallel and sequential multiple mediation models. We considered two mediators in each multiple mediation model. The first mediator was always Heart PC2 (mediator 1), and we used the brain latents as the second mediator (mediator 2). In parallel multiple mediation, the mediator 1 is not explicitly considered as a predictor for mediator 2 while it is considered in sequential mediation. Therefore, $c=c'+a_1*b_1+a_2*b_2$ in parallel mediation, and $c=c'+a_1*b_1+a_2*b_2+a_1*m*b_2$ in sequential mediation, where ***m*** is the coefficient of the mediator 2 regressed on mediator 1. Comparing the indirect effect from the parallel multiple mediation to the single mediation allows for one to assess how unique the g associations for mediator 1 and mediator 2 are. Similarly, comparing the parallel multiple mediation and the sequential multiple mediation allows one to assess the uniqueness of the gVRF association for mediator 2. In other words, parallel multiple mediation measures how much mediator 1 mediates the association between gVRF and mediator 2.

Packages

For gVRF, g, gMD, and gFA extraction, we performed confirmatory factor analysis (CFA) using 'cfa' from the lavaan R package (Rosseel, 2012). For PCA of the CMR radiomics and brain IDPs, we used prcomp of the base R stats package. We performed CCA using 'CCA' from the scikit-learn cross-decomposition module in Python (Pedregosa et al., 2011). We performed all linear modelling with lavaan in R and report bootstrapped estimates of confidence intervals, method previously reported (Rosseel, 2012). We control for multiple hypothesis testing across all linear models by performing a Benjamini-Hochberg False Discovery Rate (BH-FDR) adjustment for all latent variable p-values (Benjamini & Hochberg, 1995). We performed propensity score matching using 'matchit' (Ho et al., 2011). We used a logistic regression distance metric and a calliper of 0.05. We matched men and women separately and then recombined. For the mediation models, we performed fitting and bootstrapping via lavaan in R and report the direct

effect, indirect effects, total effect, and percent mediation (Rosseel, 2012). In all models, we adjusted for sex and age, report both raw and deconfounded results, and correct for multiple hypothesis testing via a BH-FDR correction.

References

Alfaro-Almagro, F., Jenkinson, M., Bangerter, N. K., Andersson, J. L. R., Griffanti, L., Douaud, G., Sotiropoulos, S. N., Jbabdi, S., Hernandez-Fernandez, M., Vallee, E., Vidaurre, D., Webster, M., McCarthy, P., Rorden, C., Daducci, A., Alexander, D. C., Zhang, H., Dragonu, I., Matthews, P. M., … Smith, S. M. (2018). Image processing and Quality Control for the first 10,000 brain imaging datasets from UK Biobank. *NeuroImage*, *166*, 400–424.

Attar, R., Pereañez, M., Gooya, A., Albà, X., Zhang, L., de Vila, M. H., Lee, A. M., Aung, N., Lukaschuk, E., Sanghvi, M. M., Fung, K., Paiva, J. M., Piechnik, S. K., Neubauer, S., Petersen, S. E., & Frangi, A. F. (2019). Quantitative CMR population imaging on 20,000 subjects of the UK Biobank imaging study: LV/RV quantification pipeline and its evaluation. *Medical Image Analysis*, *56*, 26–42.

Bai, W., Sinclair, M., Tarroni, G., Oktay, O., Rajchl, M., Vaillant, G., Lee, A. M., Aung, N., Lukaschuk, E., Sanghvi, M. M., Zemrak, F., Fung, K., Paiva, J. M., Carapella, V., Kim, Y. J., Suzuki, H., Kainz, B., Matthews, P. M., Petersen, S. E., … Rueckert, D. (2018). Automated cardiovascular magnetic resonance image analysis with fully convolutional networks. *Journal of Cardiovascular Magnetic Resonance: Official Journal of the Society for Cardiovascular Magnetic Resonance*, *20*(1), 65.

Bai, W., Suzuki, H., Huang, J., Francis, C., Wang, S., Tarroni, G., Guitton, F., Aung, N., Fung, K., Petersen, S. E., Piechnik, S. K., Neubauer, S., Evangelou, E., Dehghan, A., O'Regan, D. P., Wilkins, M. R., Guo, Y., Matthews, P. M., & Rueckert, D. (2020). A population-based phenome-wide association study of cardiac and aortic structure and function. *Nature Medicine*, *26*(10), 1654–1662.

Benjamini, Y., & Hochberg, Y. (1995). Controlling the false discovery rate: A practical and powerful approach to multiple testing. *Journal of the Royal Statistical Society*, *57*(1), 289–300.

Carré, A., Klausner, G., Edjlali, M., Lerousseau, M., Briend-Diop, J., Sun, R., Ammari, S., Reuzé, S., Alvarez Andres, E., Estienne, T., Niyoteka, S., Battistella, E., Vakalopoulou, M., Dhermain, F., Paragios, N., Deutsch, E., Oppenheim, C., Pallud, J., & Robert, C. (2020). Standardization of brain MR images across machines and protocols: bridging the gap for MRI-based radiomics. *Scientific Reports*, *10*(1), 12340.

Cox, S. R., Lyall, D. M., Ritchie, S. J., Bastin, M. E., Harris, M. A., Buchanan, C. R., Fawns-Ritchie, C., Barbu, M. C., de Nooij, L., Reus, L. M., Alloza, C., Shen, X., Neilson, E., Alderson, H. L., Hunter, S., Liewald, D. C., Whalley, H. C., McIntosh, A. M., Lawrie, S. M., … Deary, I. J. (2019). Associations between vascular risk factors and brain MRI indices in UK Biobank. *European Heart Journal*, *40*(28), 2290–2300.

Cox, S. R., Ritchie, S. J., Fawns-Ritchie, C., Tucker-Drob, E. M., & Deary, I. J. (2019). Structural brain imaging correlates of general intelligence in UK Biobank. *Intelligence*, *76*, 101376.

Cox, S. R., Ritchie, S. J., Tucker-Drob, E. M., Liewald, D. C., Hagenaars, S. P., Davies, G., Wardlaw, J. M., Gale, C. R., Bastin, M. E., & Deary, I. J. (2016). Ageing and brain white matter structure in 3,513 UK Biobank participants. *Nature Communications*, *7*, 13629.

Ho, D., Imai, K., King, G., & Stuart, E. A. (2011). MatchIt: Nonparametric Preprocessing for Parametric Causal Inference. *Journal of Statistical Software*, *42*, 1–28.

MacKinnon, D. P., Fairchild, A. J., & Fritz, M. S. (2007). Mediation analysis. *Annual Review of Psychology*, *58*, 593–614.

Pedregosa, F., Varoquaux, G., Gramfort, A., Michel, V., Thirion, B., Grisel, O., Blondel, M., Prettenhofer, P., Weiss, R., Dubourg, V., & Others. (2011). Scikit-learn: Machine learning in Python. *The Journal of Machine Learning Research*, *12*, 2825–2830.

Penke, L., Muñoz Maniega, S., Murray, C., Gow, A. J., Hernández, M. C. V., Clayden, J. D., Starr, J. M., Wardlaw, J. M., Bastin, M. E., & Deary, I. J. (2010). A general factor of brain white matter integrity predicts information processing speed in healthy older people. *The Journal of Neuroscience: The Official Journal of the Society for Neuroscience*, *30*(22), 7569–7574.

Petersen, S. E., Aung, N., Sanghvi, M. M., Zemrak, F., Fung, K., Paiva, J. M., Francis, J. M., Khanji, M. Y., Lukaschuk, E., Lee, A. M., Carapella, V., Kim, Y. J., Leeson, P., Piechnik, S. K., & Neubauer, S. (2017). Reference ranges for cardiac structure and function using cardiovascular magnetic resonance (CMR) in Caucasians from the UK Biobank population cohort. *Journal of Cardiovascular Magnetic Resonance: Official Journal of the Society for Cardiovascular Magnetic Resonance*, *19*(1), 18.

Petersen, S. E., Matthews, P. M., Francis, J. M., Robson, M. D., Zemrak, F., Boubertakh, R., Young, A. A., Hudson, S., Weale, P., Garratt, S., Collins, R., Piechnik, S., & Neubauer, S. (2016). UK Biobank's cardiovascular magnetic resonance protocol. *Journal of Cardiovascular Magnetic Resonance: Official Journal of the Society for Cardiovascular Magnetic Resonance*, *18*(1), 1–7.

Raisi-Estabragh, Z., Harvey, N. C., Neubauer, S., & Petersen, S. E. (2021). Cardiovascular magnetic resonance imaging in the UK Biobank: a major international health research resource. *European Heart Journal Cardiovascular Imaging*, *22*(3), 251–258.

Raisi-Estabragh, Z., Jaggi, A., Gkontra, P., Mccracken, C., Aung, N., Munroe, P. B., Neubauer, S., Harvey, N. C., Lekadir, K., & Petersen, S. E. (2021). Cardiac magnetic resonance radiomics reveal differential impact of sex, age, and vascular risk factors on cardiac structure and myocardial tissue. *Frontiers in Cardiovascular Medicine*, *8*, 1972.

Rosseel, Y. (2012). lavaan: An R Package for Structural Equation Modeling. *Journal of Statistical Software*, *48*, 1–36.

van Timmeren, J. E., Cester, D., Tanadini-Lang, S., Alkadhi, H., & Baessler, B. (2020). Radiomics in medical imaging-"how-to" guide and critical reflection. *Insights into Imaging*, *11*(1), 91.

Supplementary Figures

Supplementary Figure 1

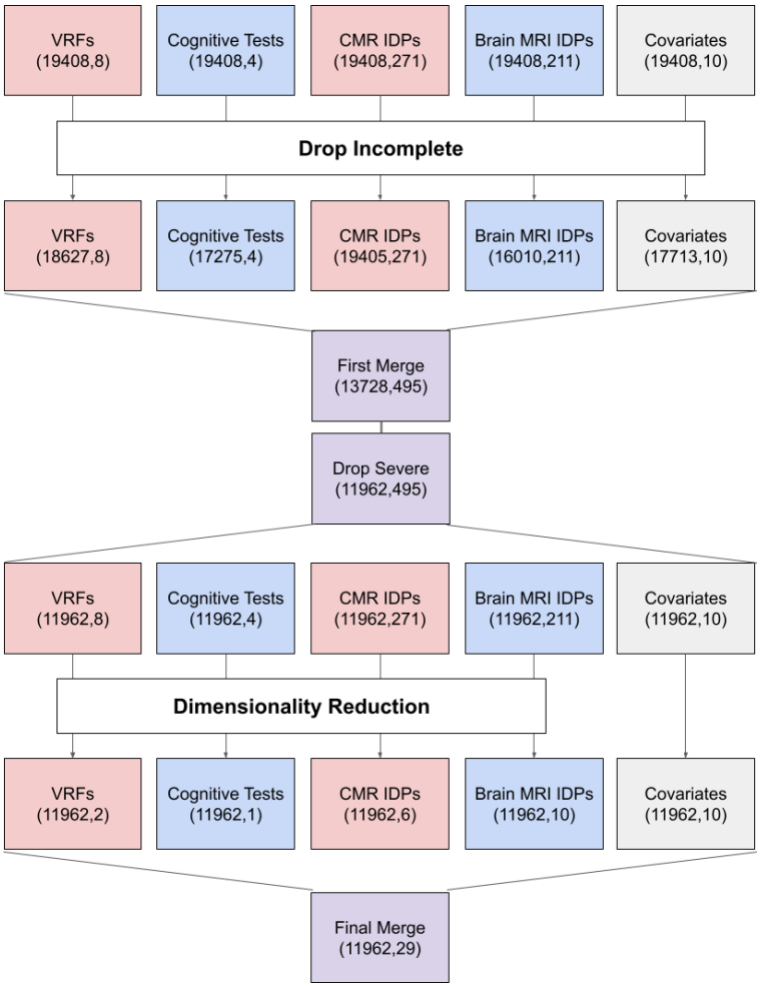

Supplementary Figure 1: Data Preparation Workflow

The flow of subjects and variables through data preparation. Each box represents the number of subjects and the number of variables after the most recent action was taken. We began with 19408 subjects with complete CMR imaging and pulled their data for the other categories. We then dropped incomplete subjects for each category and removed all subjects with a severe cardiovascular or brain disease diagnosis. We then separately conducted factor analysis (and joint factor analysis not illustrated here for clarity) and finally merged all latent variables and covariates for downstream modelling. Characteristics of final cohort in **Supplementary Table 1**.

Supplementary Figure 2

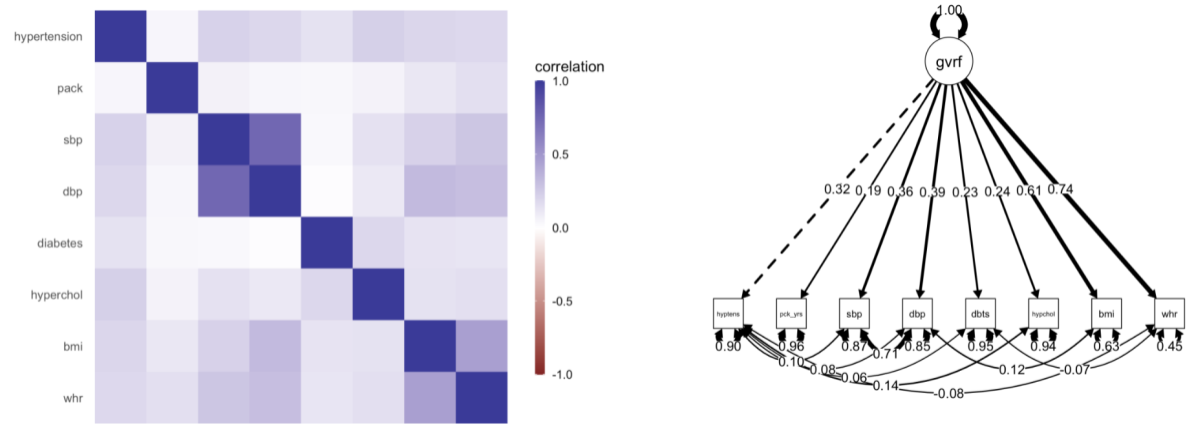

Supplementary Figure 2: CFA for Vascular Risk

A correlation heatmap and factor loadings for all vascular risk variables. Fit measures reported in **Supplementary Table 2**.

Supplementary Figure 3

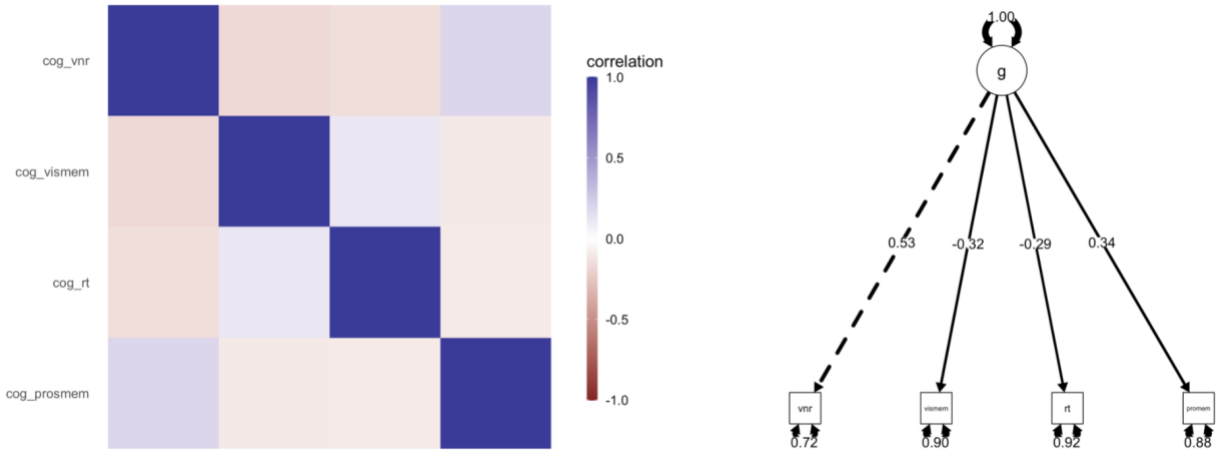

Supplementary Figure 3: CFA for Cognitive Function

A correlation heatmap and factor loadings for the cognitive exams. Fit measures reported in **Supplementary Table 3**.

Supplementary Figure 4

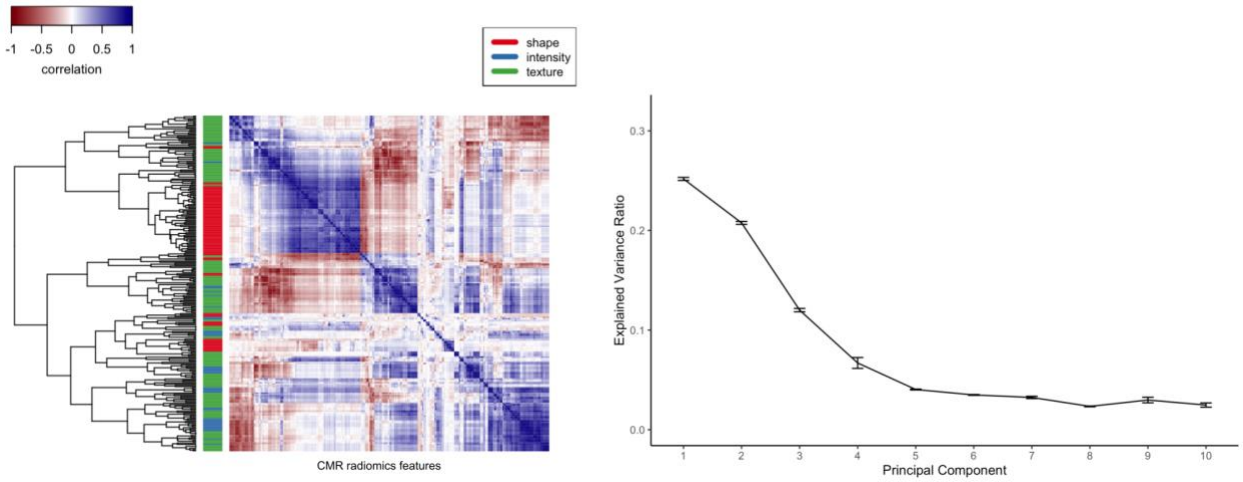

Supplementary Figure 4: PCA for CMR Radiomics

A correlation heatmap of CMR Radiomics features (sorted by a complete linkage dendrogram) with a colorbar for the original feature type. Percent variance explained of the top ten principal components of the features, error bars represent standard error over 10-fold cross validation. Individual feature loadings for each component are reported in **Supplementary Table 4**.

Supplementary Figure 5

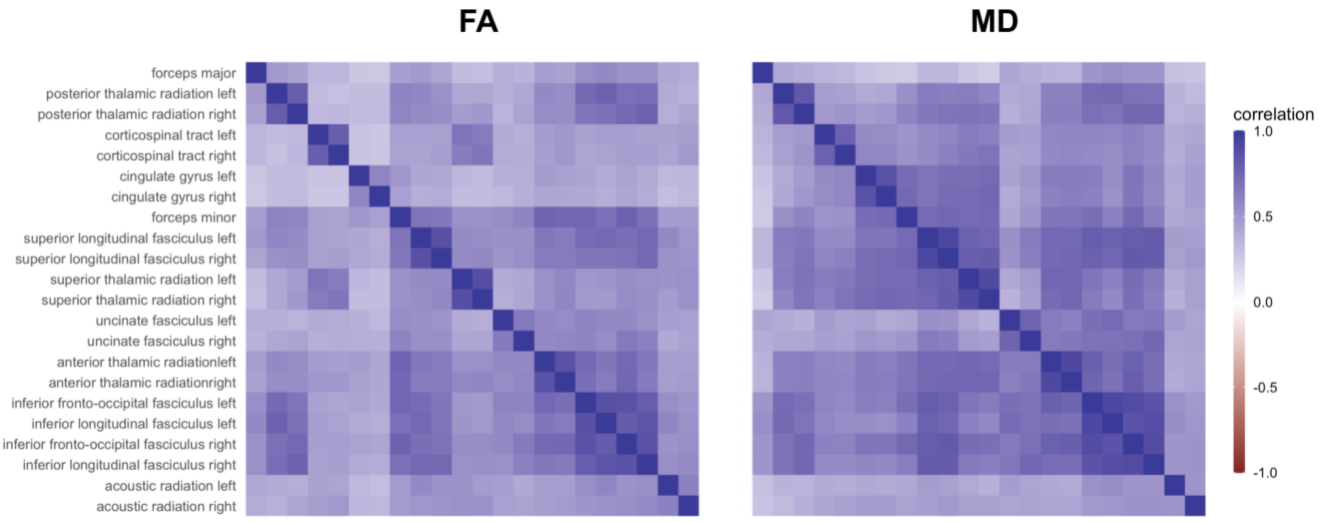

Supplementary Figure 5: CFA for FA and MD

A correlation heatmap of FA and MD IDPs. Fit measures and variable loadings are reported in **Supplementary Table 5**.

Supplementary Figure 6

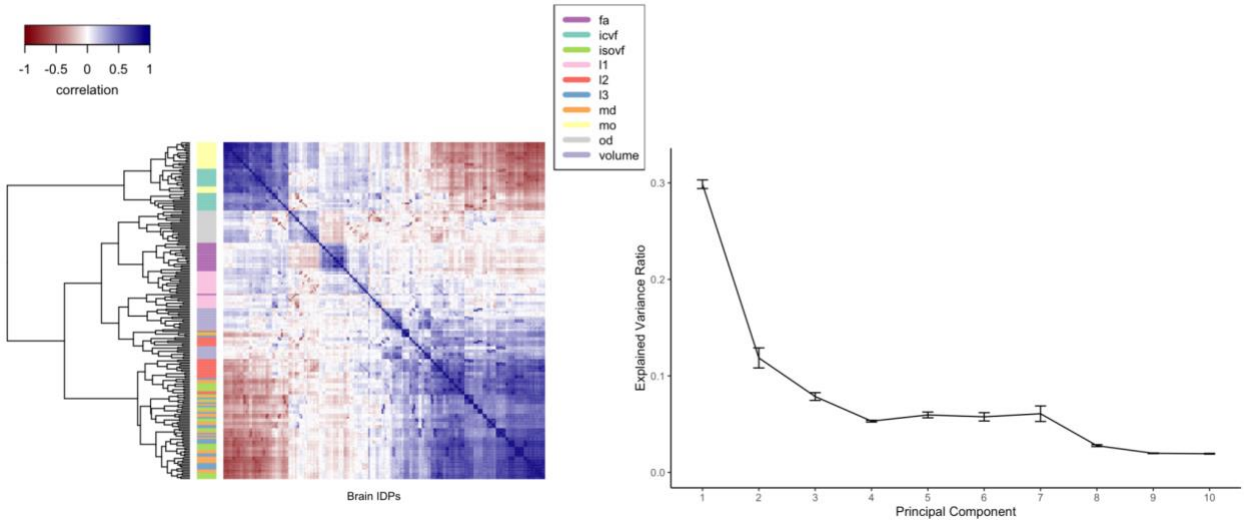

Supplementary Figure 6: PCA for Brain IDPs

A correlation heatmap of brain MR IDPs (sorted by a complete linkage dendrogram) with a colorbar for the original feature type. Percent variance explained of the top ten principal components of the features, error bars represent standard error over 10-fold cross validation. Individual feature loadings for each component are reported in **Supplementary Table 6**.

Supplementary Figure 7

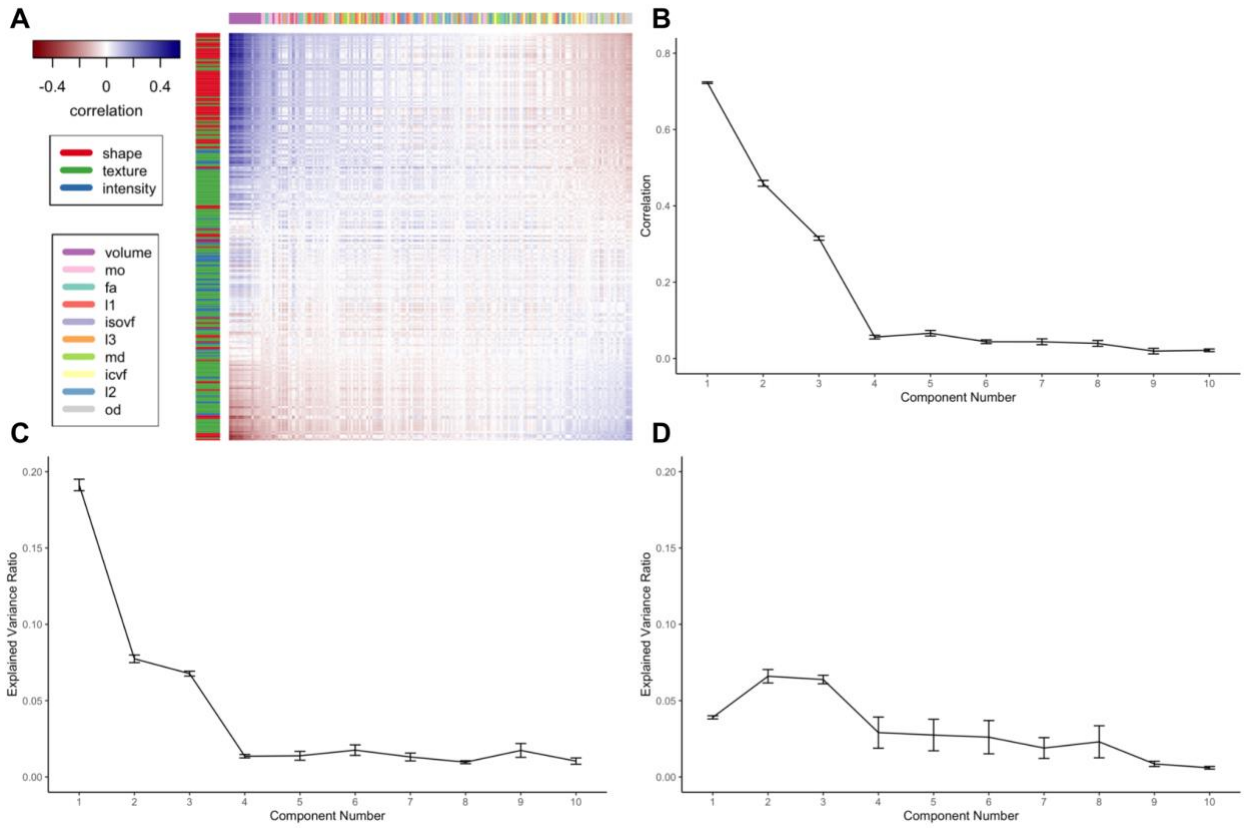

Supplementary Figure 7: CCA for Heart and Brain IDPs

(A) A correlation heatmap of the CMR Radiomics (rows) and Brain IDPs (columns). The heatmap columns and rows have been ordered by the weight of each feature in the loadings of the first CCA mode. (B) The correlation between the first ten CCA modes for the heart and brain imaging data in held-out data. The errors represent standard error over 10-fold cross validation. (C) The variance explained in held-out data by the heart component of each CCA mode. (D) The variance explained in held-out data by the brain component of each CCA mode. Individual feature loadings are reported in **Supplementary Table 7**.

Supplementary Figure 8

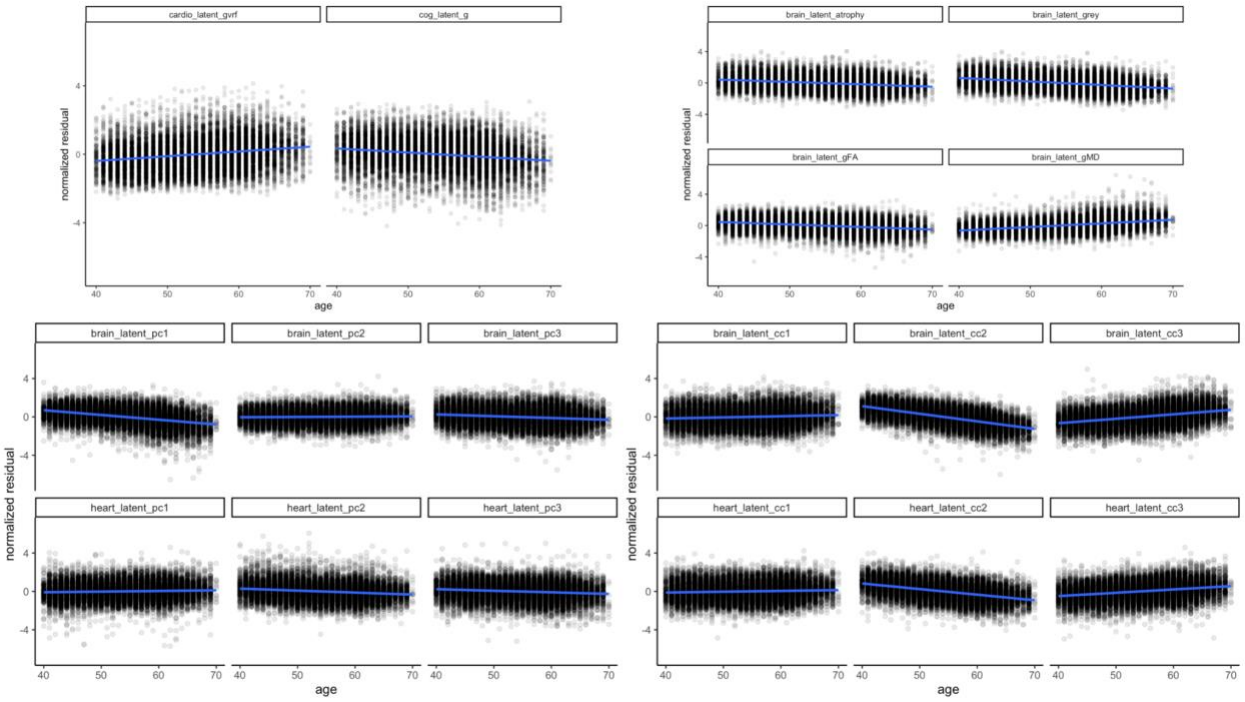

Supplementary Figure 8: Age Associations

Plot of each latent measure against age. Each latent has been deconfounded from imaging parameters as described in **Supplementary Methods**. Linear model estimates reported in **Supplementary Tables 8 and 9**.

Supplementary Figure 9

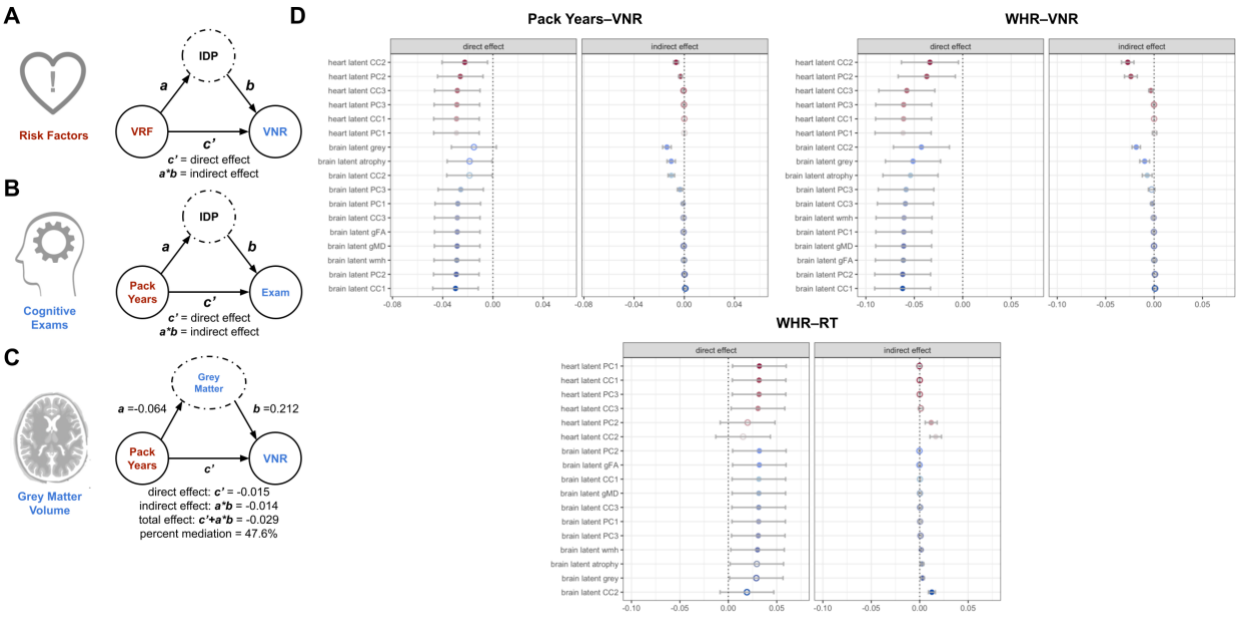

Supplementary Figure 9: Latent Single Mediation Modelling of VRF-Cognitive Pairs

We performed serial mediation modelling for all latent imaging measures for each VRF-cognitive exam pair. (A) Schematic for a mediation model using different VRFs as the independent variable rather than gVRF. We tested all VRFs. (B) Schematic for a mediation model using cognitive exams as the dependent variable rather than g. We tested all exams. (C) Example mediation model for an individual latent factor and an example pair of VRF and cognitive exam. Confidence intervals for all coefficient estimates in **Supplementary Table 21**. (D) Direct and indirect effects for three significant VRF-exam pairs. Latents ordered by indirect effect size and separated by organ. RT shows lower values for better performance while VNR shows higher values for higher performance.

Supplementary Figure 10

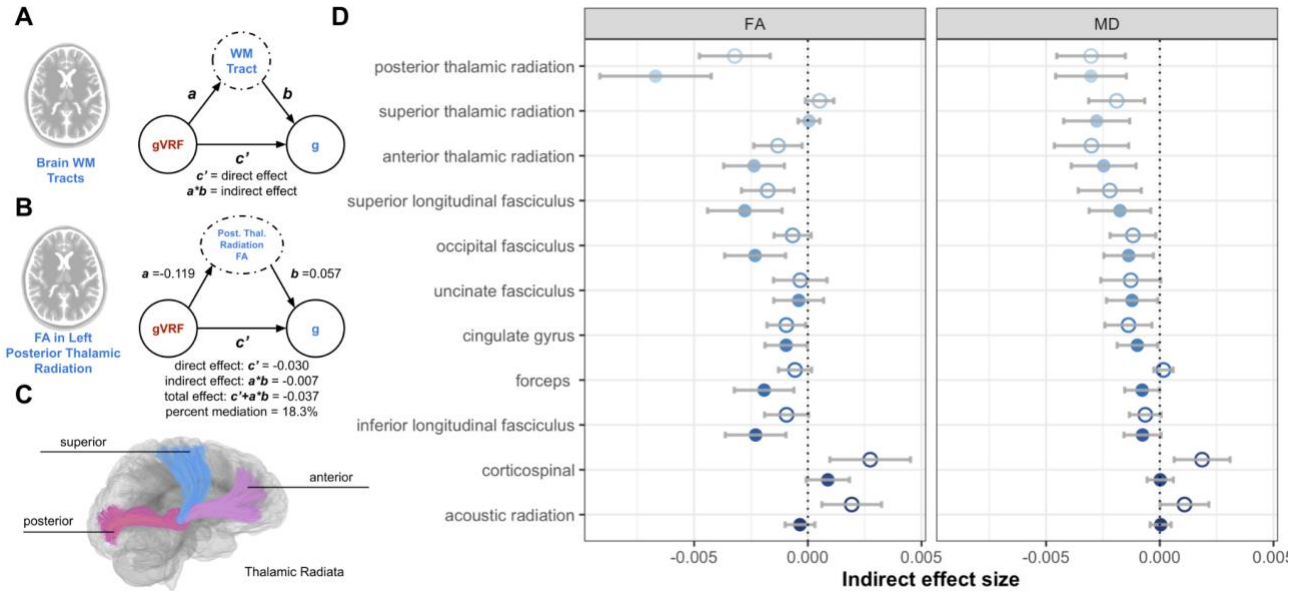

Supplementary Figure 10: White Matter Tract Mediation Modelling

We focus on serial mediation modelling for individual white matter tract quantifiers. (A) Schematic for the modelling procedure for the brain white matter tract quantifiers. (B) Example mediation model for an individual feature, fractional anisotropy of the posterior thalamic radiation. Confidence intervals reported in **Supplementary Table 25**. (C) Illustration of the key white matter tracts with large indirect effects for both FA and MD. (D) Indirect effects for all tested FA and MD measures.

Supplementary Table Captions

Supplementary Table 1: Summary statistics of the final cohort

Supplementary Table 2: Loadings and Fit Metrics for CFA of Vascular Risk Factors

Supplementary Table 3: Loadings and Fit Metrics for CFA of Cognitive Exams

Supplementary Table 4: PCA Loadings for CMR Radiomics

Supplementary Table 5: Loadings and Fit Metrics for CFA of Fractional Anisotropy and Mean Diffusivity

Supplementary Table 6: PCA Loadings for all Brain MRI IDPs

Supplementary Table 7: CCA Loadings for CMR Radiomics and Brain MRI IDPs

Supplementary Table 8: Association of each Latent Factor with Age and Sex, Raw

Supplementary Table 9: Association of each Latent Factor with Age and Sex, Deconfounded

Supplementary Table 10: Coefficients and Metrics for Pairwise Linear Modelling of all Latents, Raw

Supplementary Table 11: Coefficients and Metrics for Pairwise Linear Modelling of all Latents, Deconfounded

Supplementary Table 12: Propensity Score Matching t-tests

Supplementary Table 13: Single Mediation Model Coefficients and Metrics for all Latents, Raw, lhs: left hand side, op: operation, rhs: right hand side, est.std: standardised estimate

Supplementary Table 14: Single Mediation Model Coefficients and Metrics for all Latents, Deconfounded

Supplementary Table 15: Association of BMI with Heart PC2 controlling for heart size, mediation of the BMI-VNR association by Heart PC2, and mediation of the gVRF-g association by Heart PC2 covarying for BMI

Supplementary Table 16: Multiple Parallel Mediation Model Coefficients and Metrics for all Latents, Raw

Supplementary Table 17: Multiple Parallel Mediation Model Coefficients and Metrics for all Latents, Deconfounded

Supplementary Table 18: Multiple Sequential Mediation Model Coefficients and Metrics for all Latents, Raw

Supplementary Table 19: Multiple Sequential Mediation Model Coefficients and Metrics for all Latents, Deconfounded

Supplementary Table 20: Single Mediation Model Coefficients and Metrics for all Latents and all significant VRF-cognitive pairs, Raw

Supplementary Table 21: Single Mediation Model Coefficients and Metrics for all Latents and all significant VRF-cognitive pairs, Deconfounded

Supplementary Table 22: Single Mediation Model Coefficients and Metrics for all individual CMR radiomics features, Raw

Supplementary Table 23: Single Mediation Model Coefficients and Metrics for all individual CMR radiomics features, Deconfounded

Supplementary Table 24: Single Mediation Model Coefficients and Metrics for all individual Brain MRI IDPs, Raw

Supplementary Table 25: Single Mediation Model Coefficients and Metrics for all individual Brain MRI IDPs, Deconfounded

Supplementary Table 26: Single Mediation Model Coefficients and Metrics for all Bai, et al. CMR features, Deconfounded